Simulation of Solar Cell Efficiency using ATHENA and ATLAS

By

Mohd Mustaqiim bin Mohd Noor

Dissertation submitted in partial fulfillment of

the requirements for the

Bachelor of Engineering (Hons)

(Electrical & Electronics Engineering)

SEPTEMBER 2011

Universiti Teknologi PETRONAS

Bandar Seri Iskandar

31750 Tronoh

Perak Darul Ridzuan

CERTIFICATION OF APPROVAL

Simulation of Solar Cell Efficiency using ATHENA and ATLAS

by

Mohd Mustaqiim bin Mohd Noor

A project dissertation submitted to the

Electrical & Electronics Engineering Programme

Universiti Teknologi PETRONAS

in partial fulfillment of the requirement for the

Bachelor of Engineering (Hons)

(Electrical & Electronics Engineering)

Approved:

Dr. Zainal Arif bin Burhanudin

Project Supervisor

UNIVERSITI TEKNOLOGI PETRONAS

TRONOH, PERAK

December 2011

CERTIFICATION OF ORIGINALITY

This is to certify that I am responsible for the work submitted in this project, that the original work is my own except as specified in the references and acknowledgements, and that the original work contained herein have not been undertaken or done by unspecified sources or persons.

Mohd Mustaqiim bin Mohd Noor

ABSTRACT

This dissertation is to report the simulation of solar cell using ATHENA and ATLAS. The report is divided into three sections according to the objectives of the project which are to simulate the P-N Junction Solar Cell, to determine the optical properties of the materials in Dye-Sensitized Solar Cell and to simulate the efficiency of Dye-Sensitized Solar Cell at various titania, TiO_2 particle size using ATLAS.

Development of actual solar cell is costly. If the efficiency of the developed solar cell is low, it will generate low power and hence uneconomical to be practically used. Simulating the solar cell before the actual development of the solar cell can help to avoid producing solar cell with low efficiency. In this project, the scope is limited to basic P-N Junction Solar Cell and Dye-Sensitized Solar Cell. The P-N Junction Solar Cell which is the First Generation Solar Cell has been developed since 1954. Hence, the P-N Junction Solar Cell is very established and is used in this project to familiarize with ATHENA and ATLAS. Next, the project is continued to determine the optical properties of the materials in the Dye-Sensitized Solar Cell via absorption spectroscopy. The data is then used to obtain the complex refractive index for the material in order to define the properties of the materials in the ATLAS. From the obtained data, the Dye-Sensitized Solar Cell is then simulated using ATLAS.

The simulation of the basic P-N Junction Solar Cell shows that Boron doping concentration, oxide layer thickness and metal contact area plays an important role to increase the efficiency of the solar cell. However, the doping concentration of Phosphorus does not significantly affect the solar cell performance. Next, our work shows that the absorbance of the titania/dye layer is optimum at titania particle size is around 20 nm. This results into higher values of

absorption coefficient and extinction coefficient. Also, our calculation has shown that the titania particle size also affected the refractive index of the titania/dye layer. Lastly, the simulation of the Dye-Sensitized Solar Cell shows that the efficiency of the solar cell is highest when the titania particle size is at 20 nm.

In order to verify our model of the Dye-Sensitized Solar Cell, we had measured the IV characteristics of the actual Dye-Sensitized Solar Cell. The comparison shows variations between the IV characteristics of the simulated Dye-Sensitized Solar Cell and the actual solar cell. However, the results of the simulated and actual cell show the same effect when the titania particle size is varied.

ACKNOWLEDGEMENTS

First and foremost, I would like to express my appreciation to my project supervisor, Dr. Zainal Arif bin Burhanudin for his valuable input, guidance and patience throughout the course of this project. Next, I would like to thank Solar Lab members for the supports that they provided during the completion of the project especially Azela and Adel who helped me in better understanding of the Dye-Sensitized Solar Cell.

I also would like to express gratitude to Electrical and Electronics Engineering Department of Universiti Teknologi PETRONAS (UTP) for providing this chance to undertake this remarkable final year project. Thanks to all students, lecturers and technicians who had provided untiring guidance and help throughout the period of the project. Also, I would like to thanks my family and friends who are always there to support me.

Finally, I would like to apologize if any party is inadvertently excluded from being mentioned above and I would like to thank all parties that were involved in making this project a success. Thank you.

TABLE OF CONTENT

LIST OF FIGURES

LIST OF TABLES

CHAPTER 1

INTRODUCTION

1.1 Project Background

As of 2004, the solar cell market is still mainly dominated by the solar cell module based on crystalline silicon. Specifically, 36% of the market is based on single crystal meanwhile 58% of the market is based on multicrystalline silicon [12]. Only small amount of the market is based on thin film technologies. Currently the market for solar cell is increasing even though the production cost of solar cell per kW of energy generated is still large compared to other sources of electricity. From the beginning of the development of solar cells, researchers have identified the main problem for the high cost is the production cost to produce the silicon wafer. Hence, in order to cut the cost, there is a move to switch to technologies which are not based on silicon wafer to produce solar cell.

1.2 Problem Statement

The process to develop an actual solar cell is costly. Hence, only efficient solar cell is practical to be produced and used to generate electricity. When a solar cell has a low efficiency, it will generate low power. This will result into more cost in producing the same amount of power. Hence, an efficient solar cell is more attractive to be mass produced. This is because solar cell needs to compete with other cheaper means of producing electricity such as those from coal. Simulating the solar cell before the actual development of the solar cell can help to avoid producing solar cell with low efficiency. In order to test the capability of the designed solar cell, ATHENA and ATLAS can provide a simulation tool that is suitable for solar cells. ATHENA provides a mean to simulate the solar cell fabrication meanwhile ATLAS enables user to simulate the electrical, optical and thermal behaviour of the semiconductor device.

1.3 Scope of Work

This project is focused to simulate the Dye-Sensitized Solar Cell (DSSC). However, the Silicon P-N junction is also considered for familiarization purpose. In addition, the size of the TiO_2 nanoparticles in the photoanode layer of the Dye-Sensitized Solar Cell will be varied. This is achieved through varying the calcinations temperature of TiO_2. Next, the project work continues to obtain the optical properties of the Dye-Sensitized Solar Cell. The optical properties of the Dye-Sensitized Solar Cell then will be used in ATLAS to simulate the performance of the device.

1.4 Objective

The objectives of the project are

- To use ATHENA and ATLAS to simulate the First Generation Solar Cell i.e. the silicon P-N junction solar cell and to investigate the parameters that affect its efficiency.
- To determine the complex refractive index of the TiO_2/dye layer with various TiO_2 particle sizes and the electrolyte layer based on UV-Vis Absorption data
- To simulate Dye-Sensitized Solar Cell performance based on the size of the TiO_2 nanoparticles in the photoanode layer.

CHAPTER 2

LITERATURE REVIEW

The Photovoltaic Effect has been discovered by Edmond Becquerel, a French scientist back in 1839 while experimenting with an electrolytic cell. He observed the electricity generation increased when the electrolytic cell is exposed to light. Later in 1887, Heinrich Hertz discovered that ultraviolet light can change the lowest voltage that is capable of producing a spark between two metal electrodes. This effect is later described by Albert Einstein in 1905 in his paper that describes the Photoelectric Effect [18]. Both discoveries are very important to the application of solar cell. However, the first solar cell that is practical to become the source of electricity is only founded in 1954 when Daryl Chapin, Calvin Fuller and Gerald Pearson of Bell Laboratories announce their findings of the solar cell that is capable of generating electricity to be used by electrical equipments.

2.1 First Generation Solar Cell

Prior to silicon based solar cell, there were already Selenium solar cells in the market. However, the Selenium solar cell only produces 5 watts per square meter which is about 0.5% efficient. In 1954, Bell Laboratories has shown remarkable advancement when they have shown that their solar cell has reached 4% efficiency [4].

The first generation solar cells are based on diffused silicon P-N junction. The solar cell is formed by introducing specific impurities (dopants) to the silicon wafer called the doping process. Typically, the silicon wafer is doped with Boron, B to form a p-type layer. The wafer is then diffused with Phosphorus, P to produce an n-type layer and hence forming the P-N junction. In order to make contact to the P-N junction, the metal contact is screen printed to the P-N junction. The metal is then densified by firing at high temperature. Figure 1

shows the schematic of a simple solar cell which is developed in early 1960s and used for over a decade.

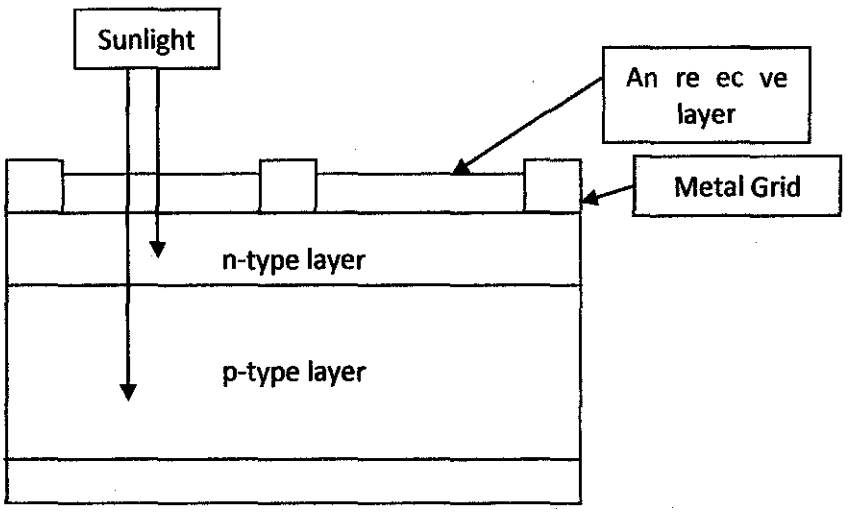

Figure 1: Schematic of a simple solar cell [11].

In order to further understand the solar cell, the basic building block of the solar cell which is the P-N junction is further analysed. A P-N junction is shown in Figure 2. The P-N junction is formed when a p-type layer (majority carriers are holes) is made contact to an n-type layer (majority carriers are electrons). The difference of the majority carrier type forms a gradient in carrier concentrations. This leads the holes from the p-type layer to diffuse to the n-type layer, and the electrons from the n-type layer to diffuse to the p-type layer. In the diffusion process, the carriers will recombine. The recombination of the holes and electrons forms the depletion region (space charge region). The diffusion of electrons leaves positive ions at the n-type layer. Meanwhile the diffusion of holes leaves negative ion at the p-type layer. The electric field (electrostatic potential difference) formed then limits the diffusion of the carriers [6].

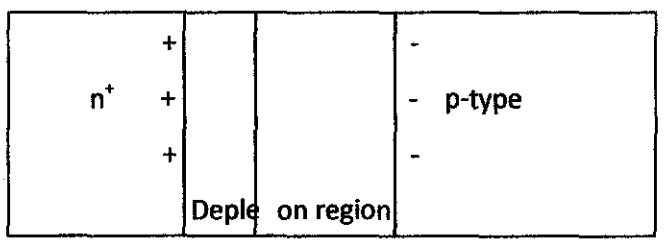

Figure 2: P-N junction model.

The more heavily doped region is called the emitter (n-type layer, usually very thin layer) and the lightly doped region is called the base or absorber region (p-type layer). This is because light absorption mostly occurs in the base hence the name absorber region. The sunlight absorption in the solar cell caused the electron in the valence band to be excited to the conduction band (leaving behind holes). The total energy and momentum, of all particles involved in the absorption process must be conserved. The photon momentum, $p_\lambda = h/\lambda$ is very small compared to the range of crystal momentum, $p = h/l$ (note that λ is the order of 10^{-6}m, meanwhile the lattice constant, l is in the order of 10^{-10}m). This means that the photon momentum will conserve the momentum of electron. It is given that the absorption coefficient for a given photon energy ($E = hv$) is proportional to probability of transition of an electron from initial state to the final state (P_{12}), the density of electrons in the initial state, E_1 and the density of available final state, E_2 and then summed over all transition between states where band gap is equal to photon energy E_2-E_1=hv [12].

The first generation solar cell is a high efficiency and high cost solar cells. Most of the cost for this type of solar cell comes from the production cost of Silicon wafer that has a very strict specification on the level of impurities. The process is also very energy intensive. The problem is reduced when there is a lower specification of impurities in the Silicon wafer used for the production of solar cell. The wafer is regarded as solar grade silicon wafer. The cost will be reduced further more by usage of thinner wafer, more efficient use of Silicon, Si and an increase of the efficiency of the solar module before 2020 [12]. However, the material cost will eventually increase and hence the need for development of the second generation solar cell which have cost advantage to the first generation solar cell because of the reduced material usage and large processing area [12].

2.2 Second Generation Solar Cell

The second generation solar cell is based on the thin film solar cell. Thin film thickness may vary from a few nanometer to tens of micrometers which is a large scale. Hence it is defined by the process of creating the cell. A thin film is a material created from the beginning by the random nucleation and growth

processes of individually condensing/reacting atomic/ionic /molecular species on a substrate [8]. Thin film solar cell takes the basic principle of a solar cell which is to place two electronically dissimilar materials with a thin electronic barrier in between them to separate the charges. Figure 3 shows typical thin film solar cell structures.

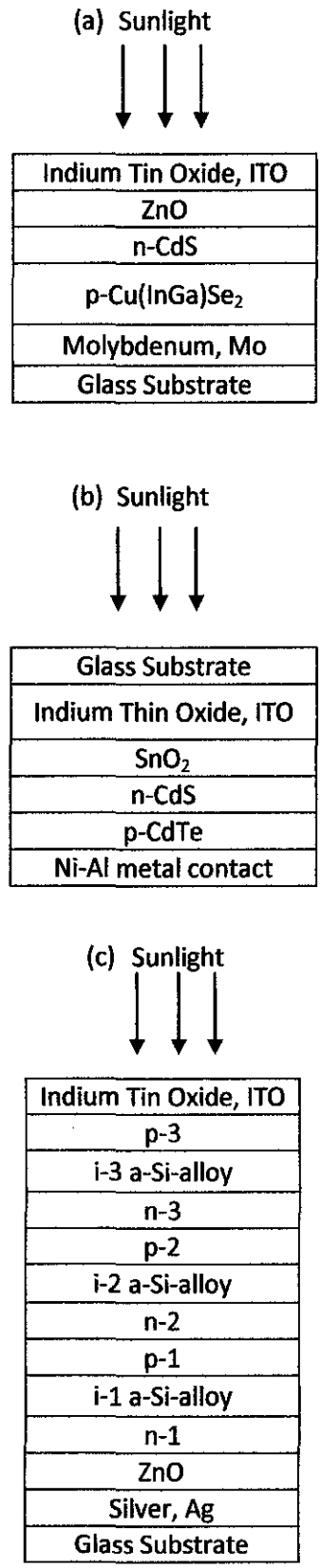

Figure 3: Typical thin film solar cell structures for single junction: (a) substrate $Cu(InGa)Se_2$, (b) superstrate CdTe, (c) tandem a-Si triple junction device [8].

However, device structures that employ mesoporous TiO_2 films change the concept of two distinctive p- and n-type layer conventionally used to form P-N junction devices. Extremely Thin Absorber (ETA) solar cells use TiO_2 mesoporous films embedded with organic and inorganic absorber materials and designed to have more effective charge carrier separation within the absorber materials and to enhance light absorption due to its scattering abilities. Figure 4 shows the innovative thin film solar cell structure.

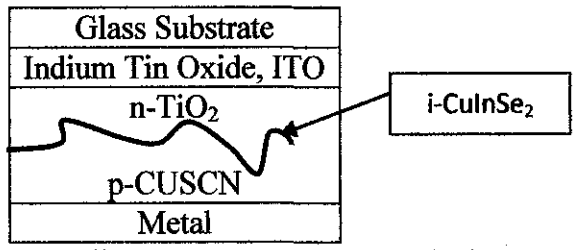

Figure 4: Innovative thin film solar cell structures: mesoporous device structures for ETA solar cell [8].

A few structures of the thin film solar cell are substrate, transparent conduction oxide (TCO), and a window. A substrate is a passive component in the solar cell. Substrate is required to be mechanically stable, matching thermal expansion coefficient with deposited layers and inert during the device fabrication.

Thin film solar cells are design to use either substrate structure or a superstrate structure. A substrate structure has a substrate of metal or metallic coating on a glass/polymer films which also act as the contact. Meanwhile, a superstrate structure has a substrate which is transparent and the contact is made by a conducting oxide coating on the substrate. A substrate structure for $Cu(InGa)Se_2$, (CIGS) solar cell has shown better efficiency than the superstrate structure. This is because of the interdiffusion of CdS during high temperature CIGS film growth.

Transparent Conducting Oxide (TCO) in general is an n-type degenerate semiconductor that has good conductivity, and high transparency. Note that it is possible to take advantage of two TCOs by forming a bilayer. The high efficiency CIGS and CdTe devices generally fabricated with a bilayer structure.

The bilayer consists of highly conducting material (for low resistance contact and lateral current collection) and highly resistive layer (which is thinner, and to minimize forward current through pinholes in the window layer).

A window layer in the heterojunction is used to form a junction with the absorber layer and to let maximum amount of light to the junction region and the absorber layer. There is no photocurrent generation occurs in the window layer. For high optical throughput with minimal losses the window layer should be very thin and have a high bandgap.

Some of the absorber used in the thin film solar cells includes the CIGS, CdTe, amorphous, micro/nanocrystalline and polycrystalline silicon and organic semiconductor. Even though the thin film solar cell has cut on cost of silicon wafer, the second generation solar cell will eventually be dominated by material cost.

2.3 Third Generation Solar Cell

A third generation solar cell is currently being developed to further decrease the cost and increase the efficiency of solar cells. The absorbed photon flux as a function of energy gap is shown in Figure 5 to demonstrate the losses of solar cell.

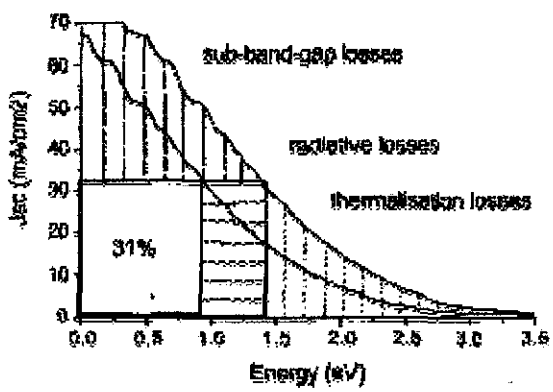

Figure 5: Absorbed photon flux as a function of energy gap. The outer curve shows absorbed photon flux as a function of energy gap at one-sun illumination. The inner curve is the work per absorbed photon as a function of absorbed photon flux. The area under the outer curve is the solar power per unit area. The

ratio of the area of the inner rectangle to the area under the outer curve gives the maximum cell efficiency for a single junction cell at one sun illumination of 31% [7].

The efficiency losses can be divided into sub-bandgap losses (photons below bandgap are not absorbed), thermalisation losses (photogenerated carriers thermalise to the band edge, losing any energy above E_g) and radiative losses. Most third generation solar cell focuses on reducing sub-bandgap and thermalisation losses in a solar cell. Radiative losses can only be reduced by elements such as optical circulators. There are a few promising approaches towards achieving more efficient solar cell including tandem cell, hot carrier cell, multilevel approaches, thermo-photovoltaic and thermo-photonic devices. This project will be focusing on the development of Dye-Sensitized Solar Cell (DSSC).

2.3.1 Dye-Sensitized Solar Cell (DSSC)

Currently, there are many researchers involves in investigating the possible advantages of devices based on mesoscopic inorganic (intermediate between microscopic and macroscopic) or organic semiconductor (carbon based compound) which is commonly referred as 'bulk' junctions due to their interconnected 3-D structure. DSSC is made with materials which offer low cost fabrication without the need for high temperature and high vacuum processes. The DSSC also opened the possibility to leave from solid state cell to devices based on interpenetrating network junctions with high conversion efficiency.

Other than that, DSSC also accomplishes the separation of optical absorption and charge separation process. This is due to the use of sensitizers as light absorbing material with a wide bandgap semiconductor. Despite being a relatively new developed technology, DSSC have been reported to achieve 11.4% efficiency. Recently, the major challenge of DSSC which is to obtain long term stability has been achieved. The basic operations of a DSSC can be summarized as in Figure 6.

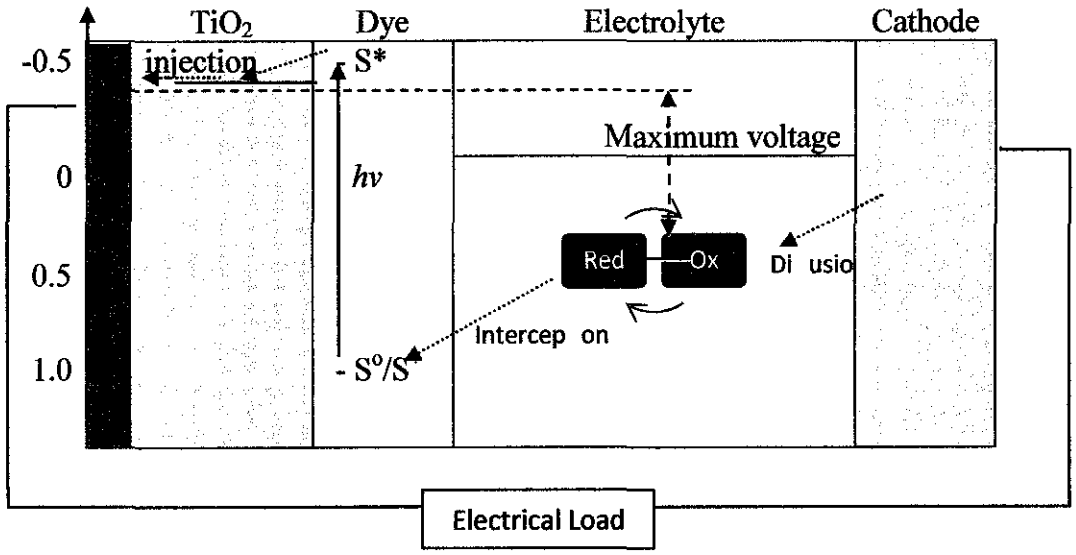

Figure 6: Energy band diagram of DSSC. Light is absorbed by the dye, S. The dye is excited, S* and injects an electron to the conduction band of a wide bandgap semiconducting oxide such as TiO_2. The electron diffuses from the semiconducting oxide to the transparent conducting glass and passes through an electrical load back to the cathode. The redox mediator is reduced by accepting an electron. The reduced mediator regenerates the sensitizer closing the cyclic conversion of light to electricity [12].

2.3.2 Optical Characteristics of Dye-Sensitized Solar Cell

As in the previous section, the dye in the DSSC is sensitized through the absorption of light. Hence, it is important to characterize the absorption of light in the DSSC in order to simulate the response of the device under illumination. In this project, the absorbance of the Dye-Sensitized Solar Cell is obtained through the measurement of UV-Vis Absorption Spectroscopy. The basic principle of UV-Vis Absorption Spectroscopy is explained through Figure 7.

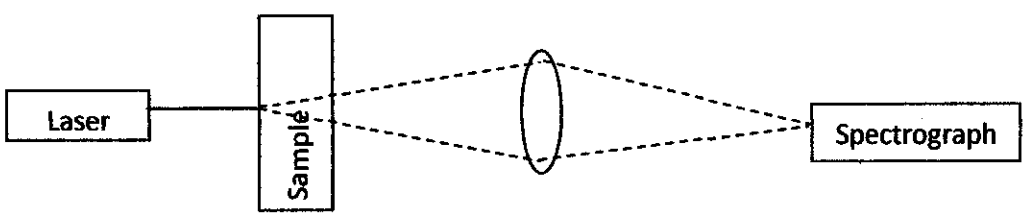

Figure 7: Basic principle of UV-Vis Absorption Spectroscopy.

The previous figure shows a beam of monochromatic radiation is being directed to the sample. The outgoing beam then is measured and recorded by the spectrograph. Hence, the incoming radiation can be compared to the outgoing radiation. The output of the Absorption Spectroscopy is absorbance, A which is given as

$$Absorbance, A = -\log_{10}\frac{I_T}{I_o} \ldots (1)$$

where I_T is the monochromatic radiant power transmitted by the sample, and I_o is the monochromatic radiant power of the incident radiation. The absorbance, A can be related to the Lambert-Beer Law [2] by the equation

$$A = -\log_{10}\frac{I_T}{I_o} = -\varepsilon dc \ldots (2)$$

where ε is the molar absorption coefficient of the sample, d is the absorption path length and c is the concentration of the sample.

The Lambert-Beer Law immediately shows that the absorbance, A of the sample is affected by the molar absorption coefficient of the sample, concentration of the sample and also the absorption path length. The absorption coefficient is a measure of the propagation distance of the optical beam into the medium before the beam is dissipated to 1/e of the initial value [17]. Absorption coefficient is given by the equation

$$I(z) = I_o e^{-\alpha z} \ldots (3)$$

where I(z) is the radiation intensity at position z, I_o is the incident radiation front surface inside the medium and α is the absorption coefficient. Hence, we can derive the absorption coefficient by the equation

$$\alpha = -\frac{1}{z} ln\left(\frac{I(z)}{I_o}\right) \ldots (4)$$

Meanwhile, the complex refractive index is given by

$$\tilde{n} = n + ik \text{ ... (5)}$$

where $\tilde{n}$ is the complex refractive index, n is the refractive index and k is the extinction coefficient. From the absorption coefficient, α we can obtain the extinction coefficient, k through the relation given by

$$k = \frac{\alpha\lambda}{4\pi} \text{ ...(6)}$$

where λ is the wavelength of the monochromatic light.

Kramers-Kronig relation describe a fundamental connection between the real and imaginary parts of linear complex optical function [19]. The relationship is given by

$$n(\omega) - 1 = \frac{2}{\pi} P \int_0^\infty \frac{\omega' \kappa(\omega')}{\omega'^2 - \omega^2} d\omega' \text{ ... (7)}$$

$$\kappa(\omega) = -\frac{2\omega}{\pi} P \int_0^\infty \frac{n(\omega') - 1}{\omega'^2 - \omega^2} d\omega' \text{ ... (8)}$$

Hence, we can estimate the real part of the complex refractive index by using the Kramers-Kronig relation. In this work, we use the approach as shown by V. Lucarini et. al. which uses MATLAB to estimate the real part of the complex refractive index. The MATLAB coding is available both from reference 19 and also from the MATLAB website.

CHAPTER 3

METHODOLOGY

The project is divided into three parts which are to simulate the silicon P-N junction solar cell, to determine the complex refractive index of the TiO_2/dye layer with various TiO_2 particle sizes and the electrolyte layer based on UV-Vis Absorption data. Next, the project work is to simulate and analyze the Dye-Sensitized Solar Cell (DSSC). In this section we will describe the methodology of the project.

3.1 Software Description and Requirement

In order to simulate the silicon solar cell efficiency, the ATHENA and ATLAS need at least the licenses for SSuprem4, S-Pisces and Luminous.

ATHENA software is used to simulate the fabrication process of the solar cell. ATHENA provides fast and accurate simulation of fabrication steps used in semiconductor technologies. SSuprem4 (used with ATHENA) is the process simulator widely used in semiconductor industry for design, analysis and optimization of Si, SiGe and compound semiconductor technologies. SSuprem4 accurately simulates major processing steps using advance physical models for diffusion, implantation, oxidation, silicidation and epitaxy.

ATLAS device simulator can extract the characteristics of a solar cell based on virtual fabrication of its physical structure. The simulator can provide output of I-V characteristics, photogeneration mapping and spectral response. The S-Pisces is used with ATLAS as a device simulator for silicon based technologies that incorporates both drift-diffusion and energy balance transport equations. The Luminous is also used with ATLAS as an advanced device module specially designed to model light absorption and photogeneration in planar and non-planar semiconductor devices. ATLAS software can simulate a more advance solar cell design features including

doping gradient, optical properties, back surface fields, back surface reflectors, windows, carrier traps, contact grid shading and complex light spectra.

3.2 Project Flowchart

The project work will be divided into two terms. The first term will be on simulating P-N junction solar cell efficiency. The main purpose for the first term is to familiarize with ATHENA and ATLAS software. Never the less, the first term will have the outcome of parameters that would be significant to the P-N junction solar cell efficiency. The second term then will be focused on determining the complex refractive index of the TiO_2/dye layer with various TiO_2 particle sizes and the electrolyte layer based on UV-Vis Absorption data. Next the project work will continue to simulate the DSSC efficiency. The project flow chart is as in Figure 8 The Gantt Chart for the project is provided in the Appendix A.

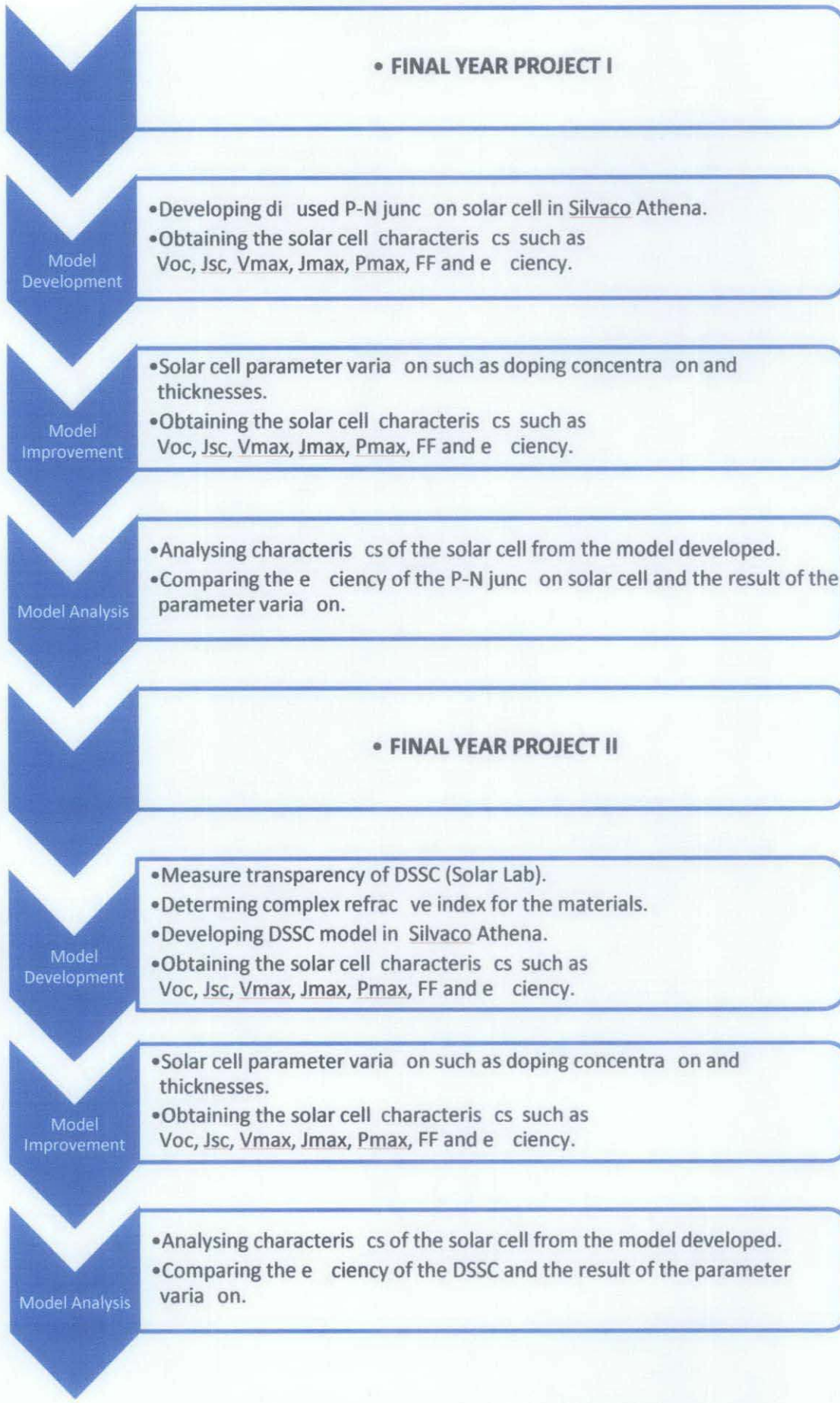

Figure 8: Flowchart of Project Methodology.

3.3 P-N Junction Solar Cell Model Development

The ATHENA software will simulate the solar cell fabrication process. In order to do so, a few basic parameters of the P-N junction solar cell must be determined. The parameters of the solar cell are summarized in Table 1. The parameters determined are then used to simulate the cell structure.

Table 1: Diffused P-N junction solar cell parameters.

Parameter	Value
Solar cell thickness	50 μm
Solar cell width	20 μm
Boron concentration, N_A	$1x10^{14}$ cm^{-3}
Phosphorus concentration, N_D	$1x\ 10^{15}$ cm^{-3}
Oxide coating thickness	0.05 μm
Front contact thickness (aluminium)	0.10 μm
Front contact width (aluminium)	4.00 μm

Figure 9 show the cell structure which is developed using parameters as defined in Table 1. The figure shows the silicon solar cell with an Aluminium metal contact (pink), and the deposited oxide layer (blue).

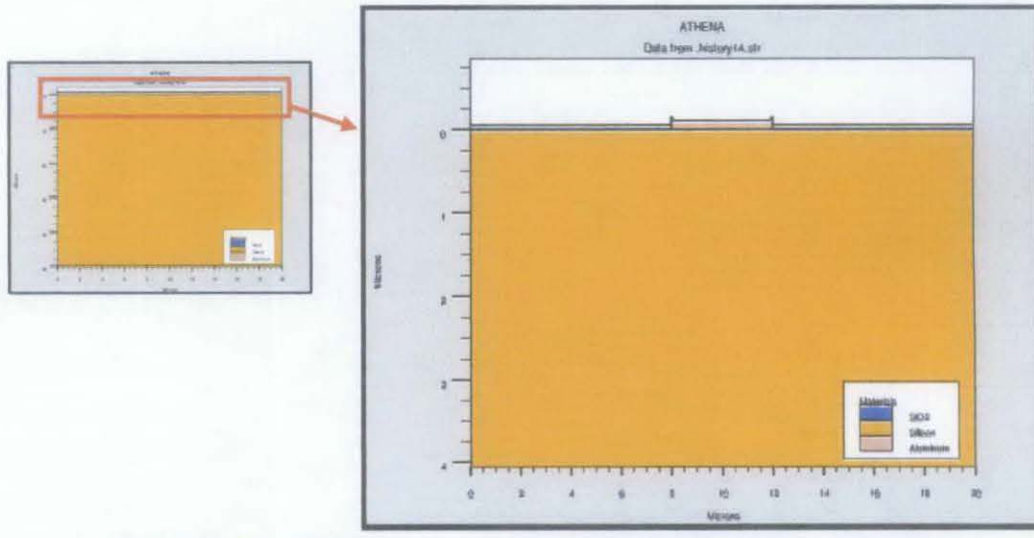

Figure 9: Zoomed in cell structure of the P-N junction solar cell.

After the fabrication process of the solar cell has been simulated using ATHENA, the response and characteristics of the solar cell will be simulated using ATLAS. In order to proceed with the simulation a few basic parameters need to be set up. The imaginary refractive index of the aluminium is set to a high value to define the metal contact as opaque to the incident sunlight (beam). The location of the beam source is

in the middle of the solar cell and 2μm from the cell. The angle of beam is 90.0° which is normal to the cell. The solar spectrum used to test the solar cell is air mass zero (AM0) which is the testing standards for solar cell which is used for aerospace application (extraterrestrial). The parameters are listed in Table 2.

Table 2: Testing parameters set up in ATLAS

Parameter	Value
Imaginary refractive index of aluminium	1000
Location of the beam source (x,y)	(10.0,-2.0)
Angle of beam	90.0°
Solar spectrum	AM0

These parameters will be used throughout the simulation process in ATLAS. The simulation is divided into three parts.

3.3.1 Short Circuit Current (Isc) and Open Circuit Voltage (Voc)

The first run of the simulation will illuminate the solar cell with the AM0 solar spectrum. The simulation will generate a log file to record the response of the solar cell. From the simulation, the short circuit current (Isc) can be extracted. Aside from that, the photogeneration rate throughout the solar cell is also being recorded in the structure file. Next the open circuit voltage will be extracted. However, in order to do so, the anode and the cathode of the solar cell need to be set as open circuit. This is done by setting cathode current as zero. The solar cell is then illuminated with the solar spectrum. The photogeneration rate and recombination rate structure file is being demonstrated in Figure 10 and Figure 11 respectively.

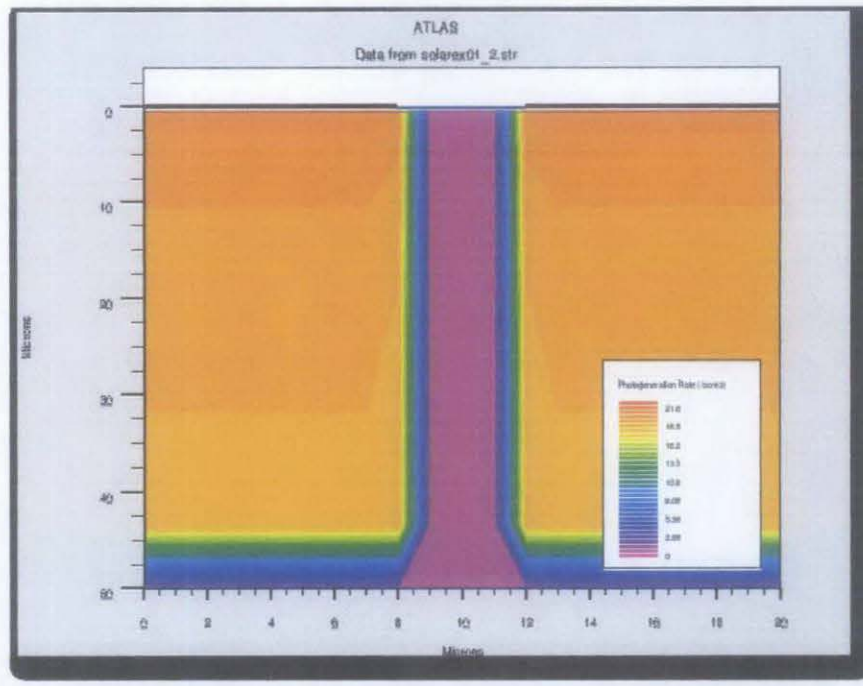

Figure 10: Photogeneration rate of the solar cell structure.

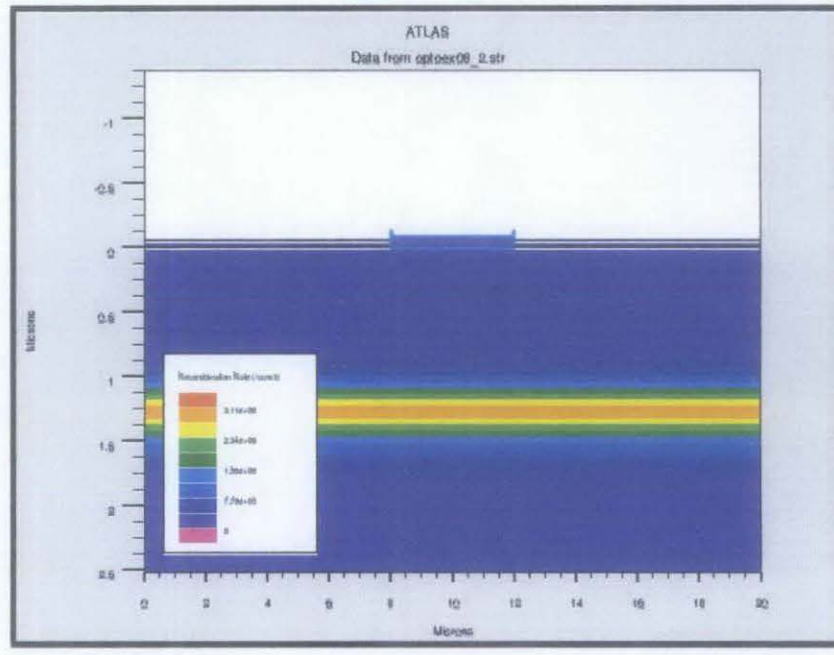

Figure 11: Recombination rate of the solar cell structure.

Both the figures show the rate (cm^{-3}) from the lowest value (magenta) to the highest value (red). The photogeneration rate and recombination rate figure will be very useful in understanding the background process of the solar cell.

3.3.2 Spectral Response

Spectral response of the solar cell is the behaviour of the solar cell under illumination with varying wavelength. In order to get the spectral response, the solar cell is being illuminated with monochromatic light beam. The wavelength of the monochromatic light beam is being sweep from 300nm to 1000nm (end of ultraviolet ray to beginning of infrared rays). The cathode current is being recorded in the log file. Figure 12 shows the spectral response of the solar cell. The green curve is the source photocurrent which is the current available in the light beam. Other than that, the red curve is the available photocurrent which is available for collection meanwhile the blue curve is the actual current that is available at the terminal.

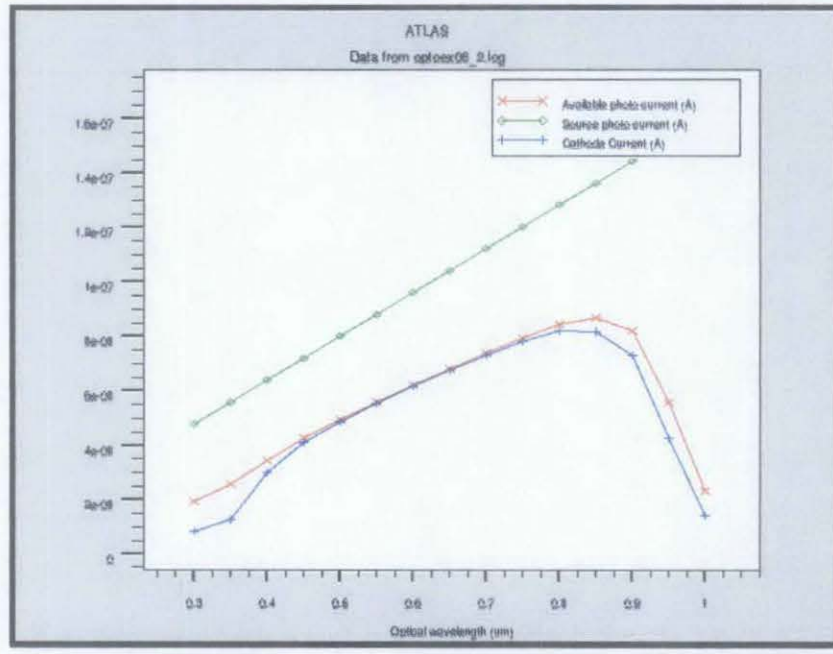

Figure 12: Spectral response of solar cell.

The losses from the source photocurrent (green curve) and the available photocurrent (red curve) is due to the reflections and transmission of the sunlight source. The losses from the available photocurrent (red curve) to the actual terminal current (blue curve) are due to the recombination of the carriers. The spectral response of the solar cell will be used to extract the Internal Quantum Efficiency (IQE) and the External Quantum Efficiency (EQE) of the solar cell. The IQE and EQE of the solar cell is given by

$$IQE = \frac{I_{anode}}{I_{available\ \ photo\ current}} \quad ...(9)$$

$$EQE = \frac{I_{anode}}{I_{source\ \ photo\ current}} \quad ...(10)$$

where I_{anode} is the current at anode terminal, $I_{available\ photo\ current}$ is the current available for collection and $I_{source\ photo\ current}$ is the current available in the light beam.

The Internal Quantum Efficiency and the External Quantum Efficiency is a function of wavelength. Both the efficiency is being plot as shown in Figure 13. The red curve is the Internal Quantum Efficiency and the green curve is the External Quantum Efficiency. The IQE shows the ratio of the current at the terminal (anode) to the current available in the beam (illumination source). Meanwhile the EQE shows the ratio of the current at the terminal (anode) to the current that is available for collection in the solar cell.

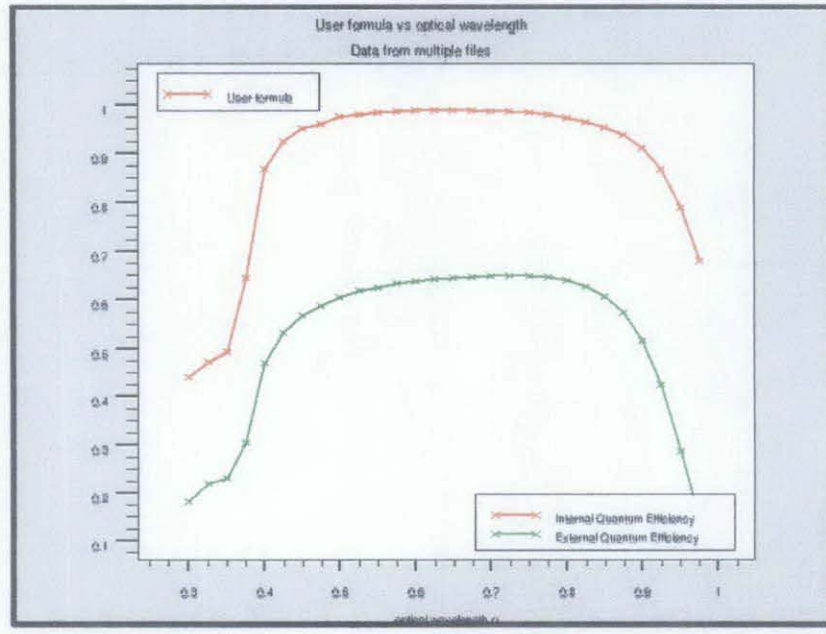

Figure 13: IQE and EQE as a function of wavelength.

3.3.3 IV Characteristics

Lastly, ATLAS is being simulated to obtain the IV characteristics of the solar cell. This is being simulated by applying voltage sweep at the cathode. The

voltage is increased from 0.01V to 1.00V. The simulation involves 2 condition; under illumination and under non-illumination (light IV characteristics and dark IV characteristics). The IV characteristics are shown in Figure 14. The green curve is the IV characteristics under illumination meanwhile the red curve is the IV characteristics with no illumination.

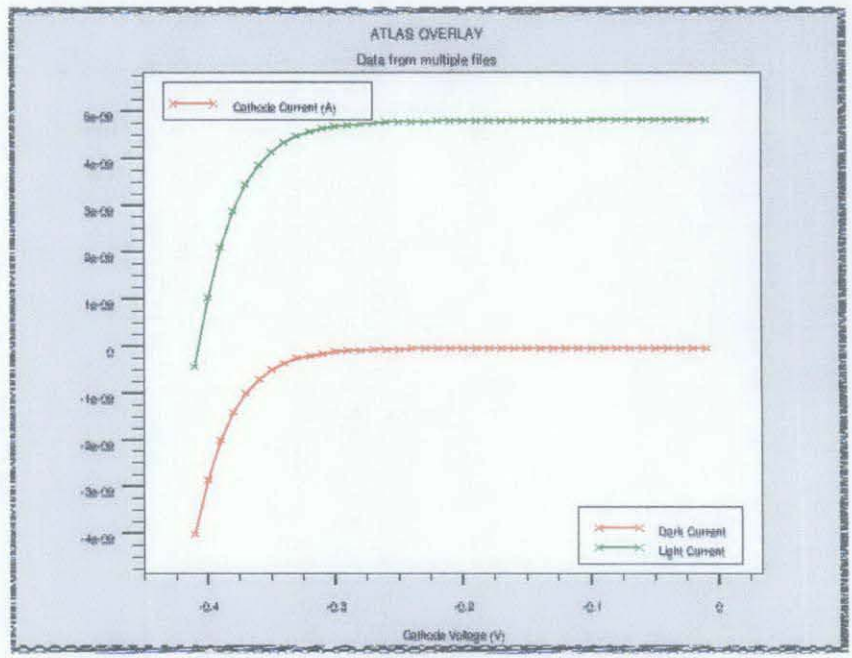

Figure 14: Dark and Light IV Characteristics.

From the Light IV characteristics, the Power versus Cathode Bias curve is extracted as shown in Figure 15. The Power, P is by:

$$P = -i_{cathode} \times v_{cathode} \quad ...(11)$$

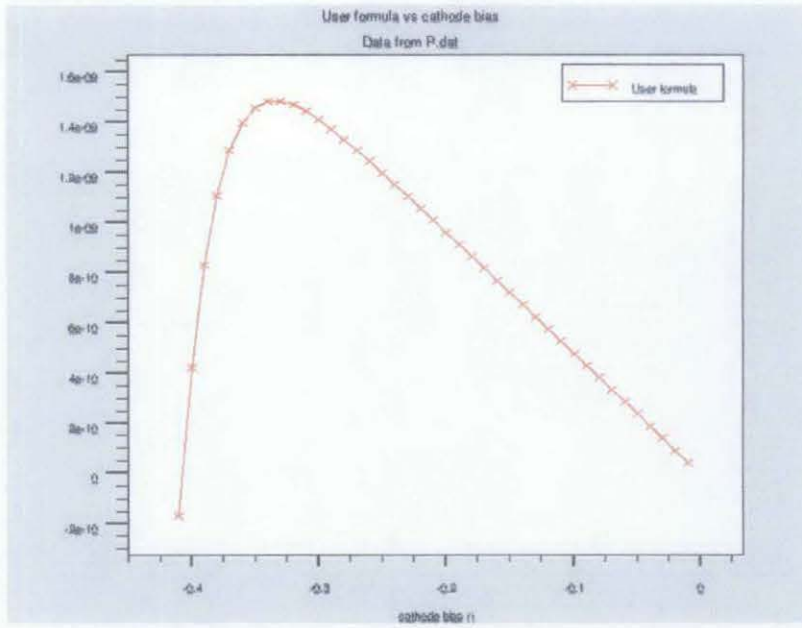

Figure 15: Power versus Cathode Bias.

From the IV characteristics, the Fill Factor, FF and Efficiency, η of the solar cell is being calculated. The Fill Factor and Efficiency is given by:

$$FF = \frac{P_{max}}{J_{sc} \times V_{oc}} \quad ...(12)$$

$$Efficiency, \eta = \frac{P_{max}}{intensity} \quad ...(13)$$

3.4 Obtaining Complex Refractive Index using UV-Vis Absorption Spectroscopy

UV-Vis spectroscopy is useful to characterize the absorption, transmission and reflectivity of a material. In this work, we obtain the absorbance, A through absorption spectroscopy measurement for the bulk heterojunction region which contains the dye adsorbed into TiO_2 nanoparticles and the iodide/triiodide electrolyte region. Figure 16 shows the flow of determining the complex refractive index of the materials.

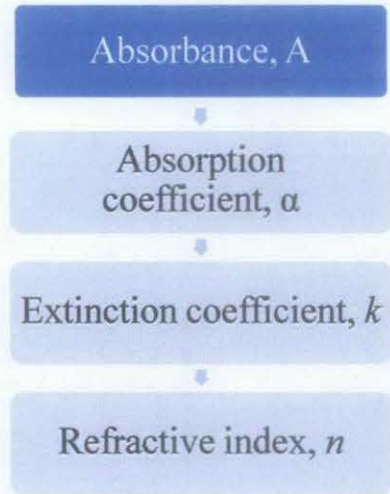

Figure 16: Flow of determining the complex refractive index of the materials.

The flow chart shows that the absorbance, A is used to obtain the absorption coefficient through equation 4. The absorption coefficient, α is then used to obtain the extinction coefficient, *k* using the relation given in equation 6. Next, we estimate the refractive index, *n* through Kramers-Kronig relation as describe in equation 7. The relation is used in MATLAB as used by Lucarini et. al.

3.5 Dye Sensitized Solar Cell Model

The Dye-Sensitized Solar Cell is defined as a device with 1 m^2 surface area with a thickness of 37 μm. The surface area is the surface that is illuminated by sunlight. Variation in the length and width of the device is ignored. Hence, the width of the device is set to be 1 μm and the length to be $1x10^{12}$ μm. Figure 1 describes the structure of the device.

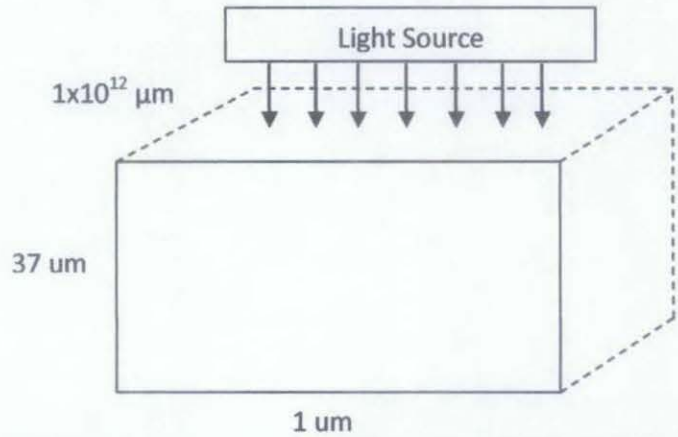

Figure 17: Dye-Sensitized Solar Cell structure defined in the ATLAS.

In this work, the device is defined to be consisting of 2 regions which are the bulk heterojunction region and the electrolyte region. The bulk heterojunction region is a 12 μm thick film containing interconnected TiO_2 nanoparticles and the light absorbing material which is the dye. Meanwhile, the electrolyte is a 25 μm thick redox mediator. In order to simulate the electrical characteristics of the device, we set the anode and the cathode to be an electrical contact with the work function of 4.4 eV. The structure of the device is shown in Figure 18.

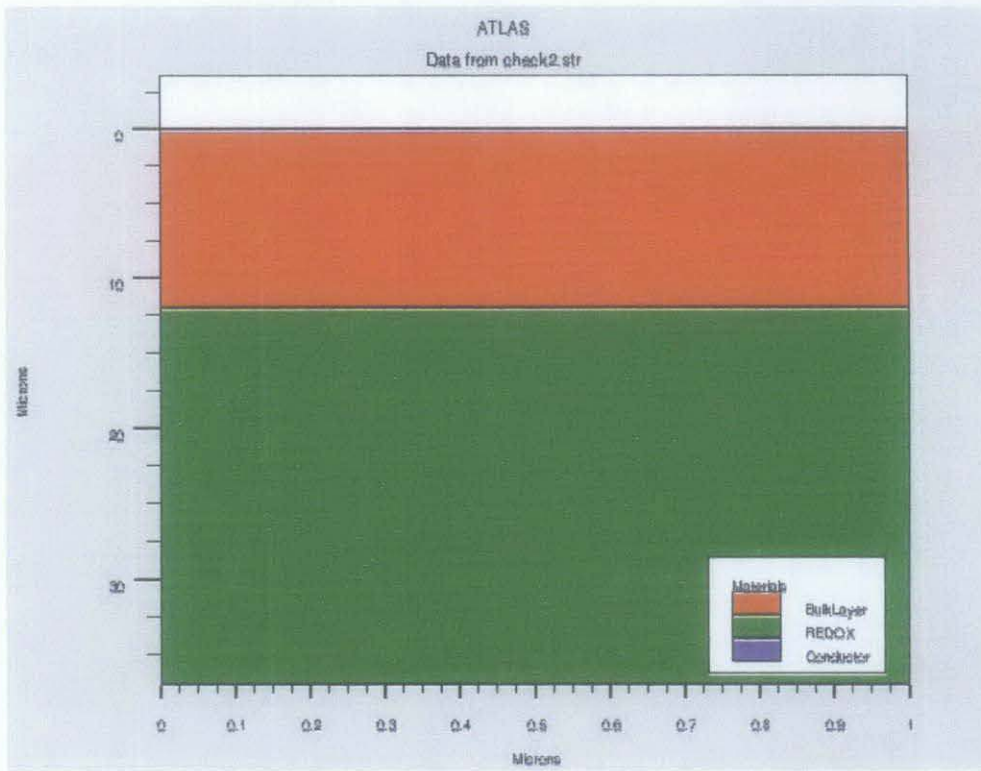

Figure 18: DSSC structure defined in ATLAS.

Next, the recombination model that is used to describe the recombination process is defined as a bimolecular process with the rate given by Langevin. Langevin recombination model is needed to enable exchange between charged carriers and singlet excitons. Hence, the model statement is used to enable the Langevin, Singlet and Singlet Dissociation model.

The material used in Dye-Sensitized Solar is not included in the default set recognized by ATLAS. Hence, the material parameters are set according to Table 3. The bulk heterojunction region contains the material named as BulkLayer and the electrolyte region contains the material named as REDOX. Other than that, the

complex refractive index of the material which is obtained through UV-Vis absorption data is also defined.

Table 3: Material Parameter defined in ATLAS.

Material	Material Parameter	Value
BulkLayer	Material Class	Semiconductor
	Permittivity	50
	Affinity	4 eV
	Energy gap	1.5 eV
	Conduction Band Density	2.8×10^{19} cm^{-3}
	Valence Band Density	1.9×10^{19} cm^{-3}
	Electron mobility	0.3 $cm^2/V.s$
	Hole Mobility	3×10^{-4} $cm^2/V.s$
REDOX	Material Class	Semiconductor
	Permittivity	3.5
	Affinity	3.4 eV
	Energy gap	0.93 eV
	Conduction Band Density	2.8×10^{19} cm^{-3}
	Valence Band Density	1.9×10^{19} cm^{-3}
	Electron mobility	7.07×10^{-2} $cm^2/V.s$
	Hole Mobility	7.07×10^{-2} $cm^2/V.s$

3.5.1 Obtaining IV Characteristics of the Dye-Sensitized Solar Cell

After the model is properly developed, ATLAS is used to simulate the dark IV and light IV characteristics of the device. In order to proceed with the simulation a few basic parameters of the source beam need to be set up. The location of the source beam is in the middle of the solar cell and 2 μm from the cell. The angle of beam is 90.0^{o} which is normal to the cell. The solar spectrum used to test the solar cell is air mass 1.5 (AM1.5) which is the standard spectrum at the earth surface. The parameters are listed in Table 4.

Table 4: Beam parameters set up in ATLAS

Parameter	Value
Location of the beam source (x,y)	(0.5,-2.0)
Angle of beam	90.0^{o}
Solar spectrum	AM1.5

Next, ATLAS is used to simulate the IV characteristics of the device is being simulated to obtain the IV characteristics of the Dye-Sensitized Solar Cell. The IV

characteristic of the Dye-Sensitized Solar Cell is obtained by setting ATLAS to perform a DC sweep from -1 V to 1 V. The DC sweep is done in two steps in order to obtain the dark IV characteristics (without illumination) and the light IV characteristics (with illumination). Figure 19 shows the dark and light IV characteristics.

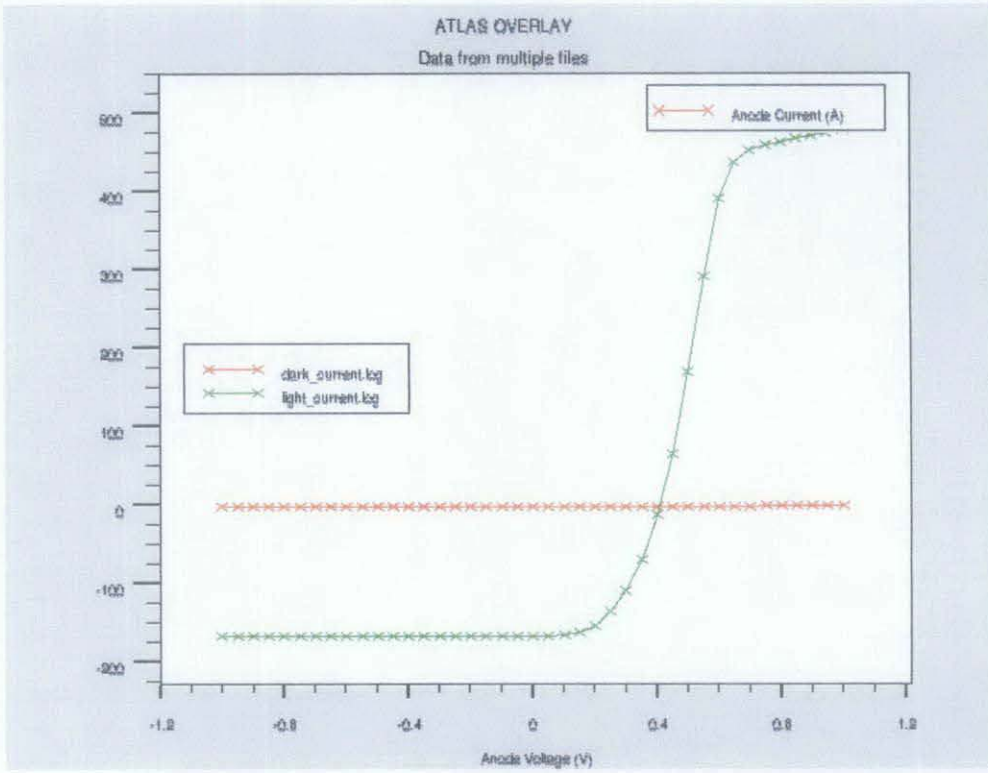

Figure 19: The dark and light IV characteristics of Dye-Sensitized Solar Cell. The red curve is the dark IV characteristics meanwhile the green curve is the light IV characteristics.

From the Light IV characteristics, the Power versus Cathode Bias curve is extracted as shown in Figure 20. The Power, P is given by:

$$P = -i_{anode} \times v_{anode} \quad ...(14)$$

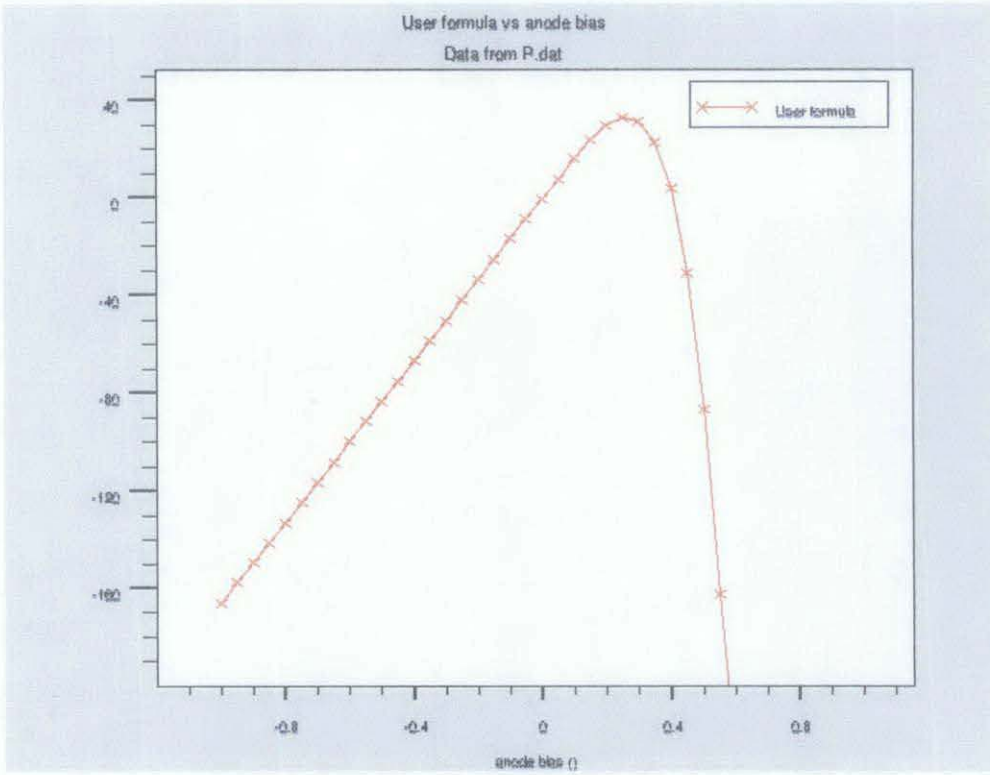

Figure 20: Power versus Anode Bias.

From the IV characteristics, the Fill Factor, FF and Efficiency, η of the Dye-Sensitized Solar Cell is also being calculated using equation 12 and 13.

CHAPTER 4

RESULTS AND DISCUSSION

As described in the previous section, the project work divided is into three parts. The first part is to simulate the silicon P-N junction solar cell. After the model of the solar cell is properly developed, we can quickly identify parameters that can be varied. In this section we will present the effect of the parameters variation. The results is tabulated and discussed. The second part is to determine the complex refractive index of the TiO_2/dye layer with various TiO_2 particle sizes and the electrolyte layer based on UV-Vis Absorption data. Here, we will present the complex refractive index variation when the TiO_2 particle size in the TiO_2/dye layer is varied. Also, we will present the electrolyte complex refractive index. The complex refractive index for the electrolyte layer is not varied. However, the complex refractive index will be used the third part of the project which is to simulate and analyze the Dye-Sensitized Solar Cell. The result of the simulation of the Dye-Sensitized Solar Cell with variation of TiO_2 particle size is also tabulated and described this section.

4.1 P-N Junction Solar Cell Parameter Variation

After collecting the data for the initial solar cell model, the parameters of the solar cell is varied. The parameters include dopants concentration (Boron and Phosphorus), oxide layer thickness, and the metal contact length. The results of the variation are tabulated in Table 5 to Table 8.

4.1.1 Boron Doping Concentrations

Table 5 shows the effect of varying the Boron doping concentration, N_A on the IV characteristics. As the dopant concentration is increased, the open circuit voltage, Voc also increases. However, the short circuit current, Jsc only increases until the concentration of $1x10^{13}$ cm^{-3}, the short circuit current, Jsc then decreases with the dopant concentration. However, due to the bigger increase in open circuit voltage, Voc, the Fill Factor and the Efficiency of the

solar cell increases with the increase of Boron doping concentration as shown in Figure 21 and 22.

Table 5: Boron Doping Concentrations Effect on IV Characteristics

Boron (cm^{-3})	Junc on Depth (um)	Short Circuit Current, Isc (A)	Open Circuit Voltage, Voc (V)	Jsc (mA/cm^2)	Pmax	Vmp p	Fill Factor	E ciency
1E+12	0.477	4.84E-09	0.26	24.21	6.82E-10	-0.18	0.54	0.026
1E+13	0.462	5.25E-09	0.33	26.24	1.10E-09	-0.25	0.63	0.042
1E+14	0.403	4.87E-09	0.41	24.33	1.49E-09	-0.33	0.75	0.057
1E+15	0.336	4.71E-09	0.47	23.55	1.75E-09	-0.40	0.79	0.066
1E+16	0.256	4.63E-09	0.53	23.15	2.00E-09	-0.46	0.81	0.076

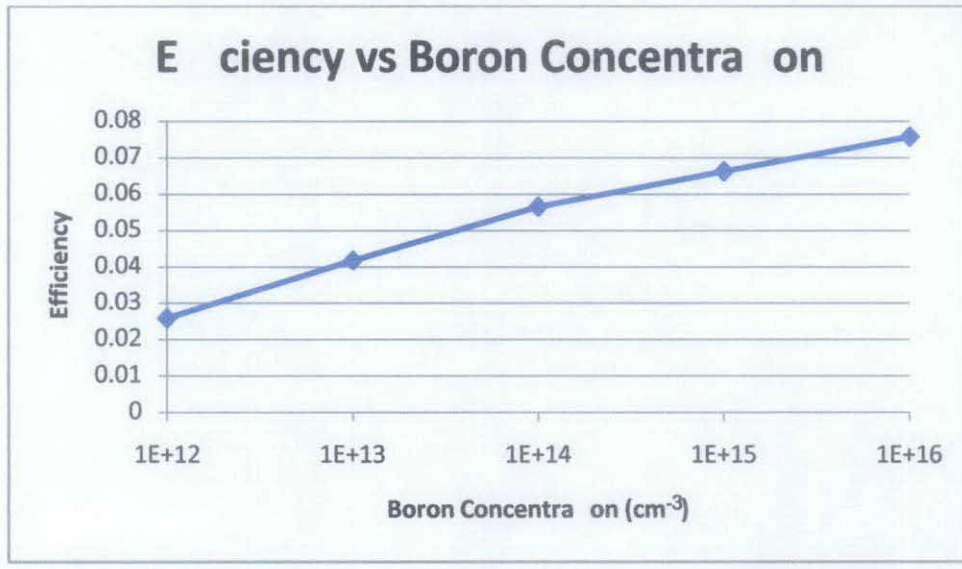

Figure 21: Boron Concentration Variation Effects on the Efficiency.

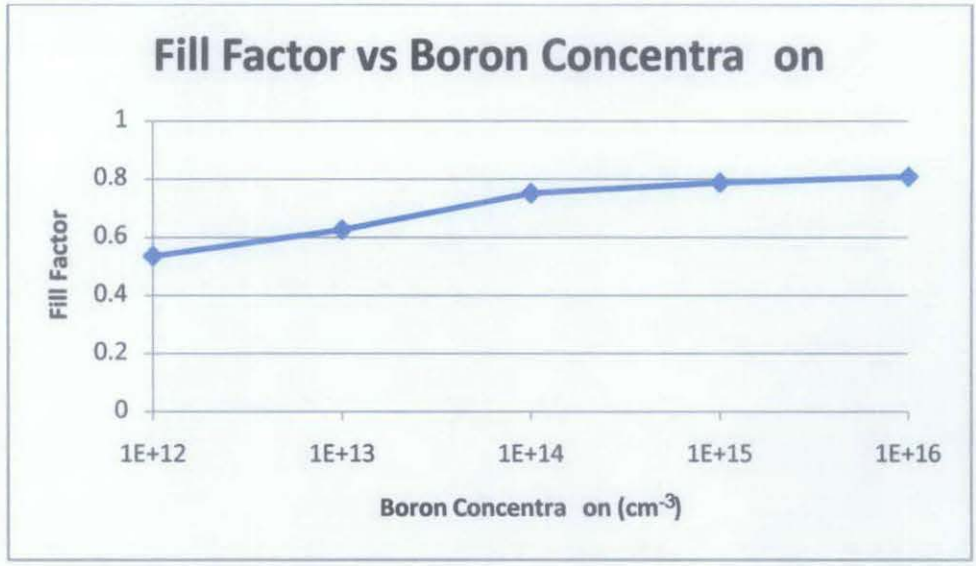

Figure 22: Boron Concentration Variation Effects on the Fill Factor.

The effect of the Boron doping concentration, N_A also shows that photogeneration rate does not show extreme changes. However, the recombination rate decreases when N_A increases. This explains the increase of the Fill Factor, FF and the Efficiency, η of the solar cell.

4.1.2 Phosphorus Doping Concentrations

Table 6 shows the effect of varying the Phosphorus doping concentration, N_D on the IV characteristics. As the dopant concentration is increased, the open circuit voltage, Voc stays at the same value. The short circuit current, Jsc also remains the same until the dopant concentration is increase to the value of of $1x10^{15}$ cm^{-3}, the short circuit current, Jsc then decreases with the dopant concentration. This shows that there is only a little change to the IV characteristics of the solar cell when the Phosphorus doping concentration is varied. However, Figure 23 shows that Phosphorus doping concentration of $1x10^{14}$ cm^{-3} will result into the most efficient solar cell. Meanwhile, the Fill Factor shows a small increment with the increase of Phosphorus doping concentration as shown in Figure 24.

Table 6: Phosphorus Doping Concentrations Effect on IV Characteristics

Phosphorus (cm^{-3})	Junc on Depth (um)	Short Circuit Current, Isc (A)	Open Circuit Voltage, Voc (V)	Jsc (mA/ cm^2)	Pmax	Vmpp	Fill Factor	E ciency
1E+12	0.237	4.87E-09	0.41	24.3	1.49 E-09	-0.33	0.75	0.056
1E+13	0.292	4.87E-09	0.41	24.3	1.49 E-09	-0.33	0.75	0.057
1E+14	0.379	4.88E-09	0.41	24.3	1.49 E-09	-0.33	0.75	0.057
1E+15	0.403	4.87E-09	0.41	24.3	1.49 E-09	-0.33	0.75	0.057
1E+16	0.416	4.77E-09	0.41	23.8	1.46 E-09	-0.33	0.75	0.055

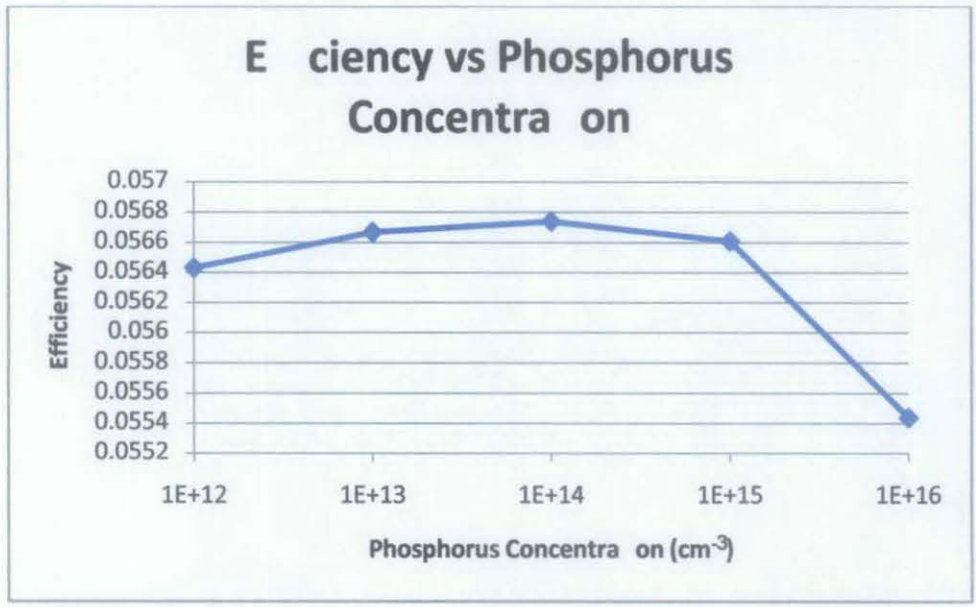

Figure 23: Phosphorus Concentration Variation Effects on the Efficiency.

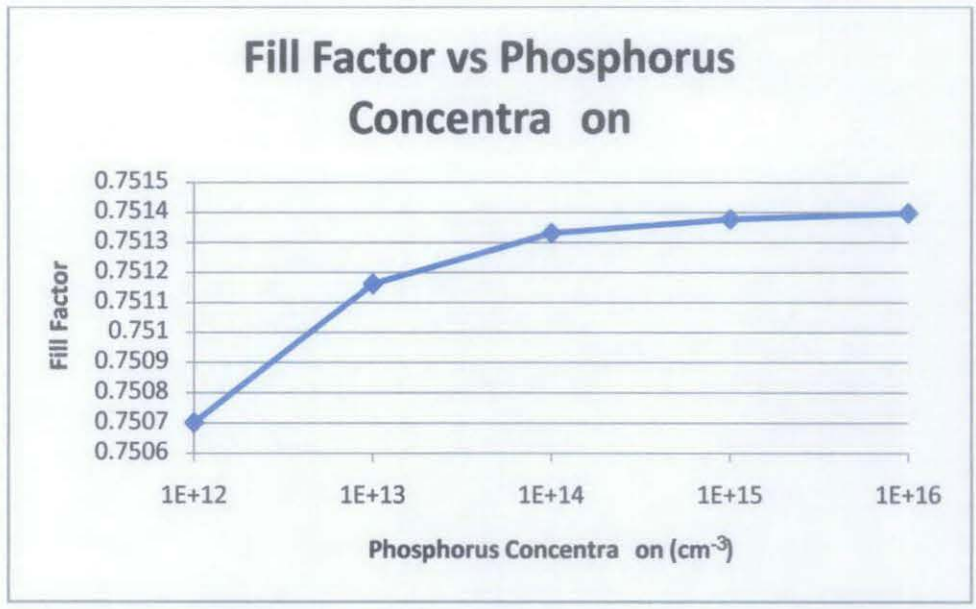

Figure 24: Phosphorus Concentration Variation Effects on the Fill Factor.

The effect of the Phosphorus doping concentration, N_D also shows that photogeneration rate does not show extreme changes. However, the recombination rate slightly decreases when N_D increases. Because there is only a small decrease of the recombination rate, the Fill Factor and the Efficiency of the solar cell only shows a small increase.

4.1.3 Oxide Layer Thickness

Table 7 shows the effect of varying the oxide layer thickness on the IV characteristics. As the oxide layer thickness is increased, the open circuit voltage, Voc is decreased together with the short circuit current, Jsc. This results into decreased Fill Factor and Efficiency as the oxide layer thickness is increased as shown in Figure 25 and 26. The oxide layer thickness decreases the Fill Factor and the Efficiency because the incoming light to the solar cell is diffused in the oxide layer.

Table 7: Oxide Layer Thickness Effect on IV Characteristics

Oxide Layer Thickness (um)	Junc on Depth (um)	Short Circuit Current, Isc (A)	Open Circuit Voltage, Voc (V)	Jsc (mA/cm^2)	Pmax	Vmpp	Fill Factor	E ciency
0.03	0.4262	4.90E-09	0.41	24.48	1.50 E-09	-0.33	0.75	0.057
0.05	0.4030	4.87E-09	0.41	24.33	1.49 E-09	-0.33	0.75	0.057
0.10	0.3230	4.82E-09	0.41	24.18	1.48 E-09	-0.33	0.75	0.056
0.20	0.0060	4.46E-09	0.27	22.32	7.58 E-10	-0.2	0.62	0.029
0.30	0.0055	4.45E-09	0.26	22.23	7.07 E-10	-0.19	0.61	0.027
0.40	0.0051	4.44E-09	0.25	22.18	6.70 E-10	-0.18	0.61	0.025

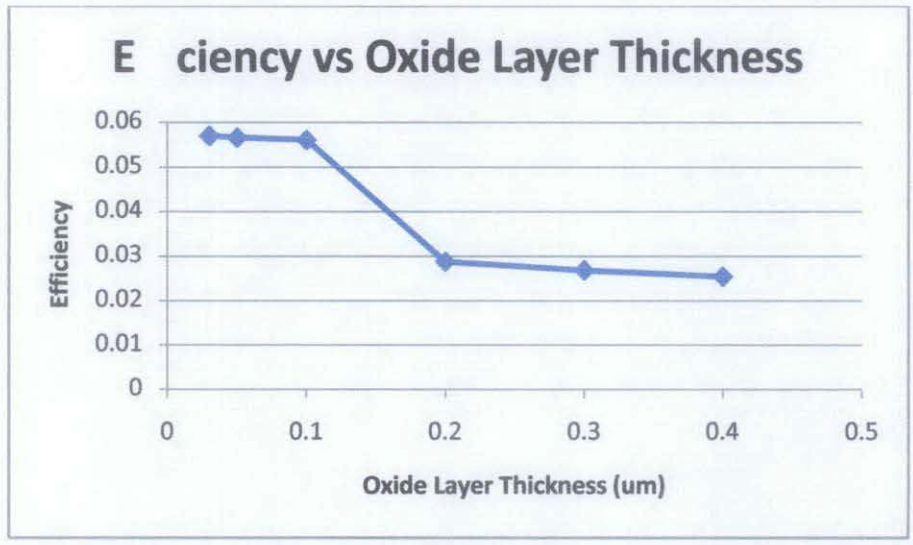

Figure 25: Oxide Layer Thickness Variation Effects on the Efficiency.

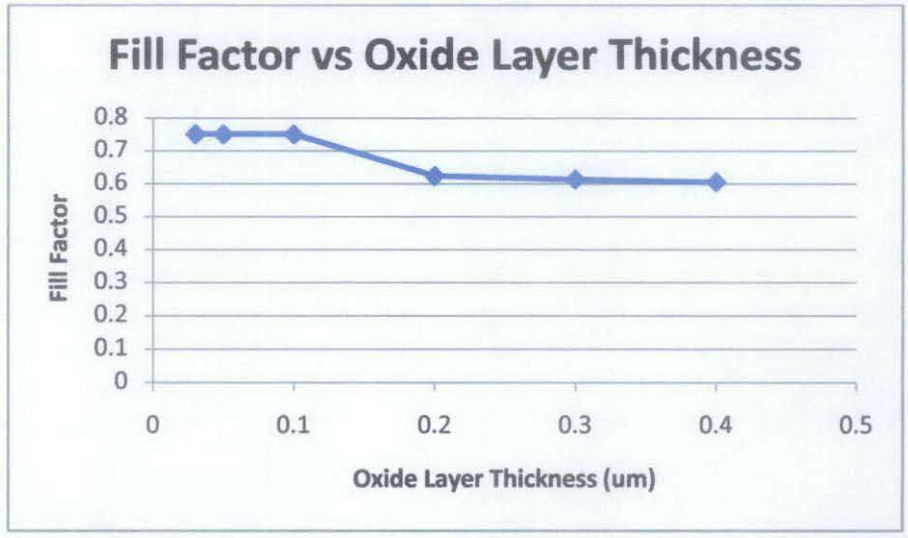

Figure 26: Oxide Layer Thickness Variation Effects on the Fill Factor.

The oxide layer thickness does not give a big impact on the photogeneration rate and the recombination rate. However, through spectral response analysis, the difference of the available photocurrent and terminal photocurrent increases when oxide layer is thicker. This shows that the there is less sunlight illumination absorbed when the oxide layer is thicker.

4.1.4 Metal Contact Length

Table 8 shows the effect of varying the metal contact length on the IV characteristics. As the metal contact length is increased, the open circuit voltage, Voc only shows a small decrement. However, the short circuit current, Jsc decreases as the metal contact length is increased. This results into the decreasing Efficiency, η of the solar cell as the metal contact length is increased as shown in Figure 27. This is due to less surface area which is directly illuminated by the sunlight. Meanwhile, the Fill Factor is relatively the same which lies around the value of 0.75 as shown in Figure 28.

Table 8: Metal Contact Length Variation Effect on IV Characteristics

Contact Length (um)	Junc on Depth (um)	Short Circuit Current, Isc (A)	Open Circuit Voltage, Voc (V)	Jsc (mA/cm^2)	Pmax	V_Pmax	Fill Factor	E ciency
2	0.403	5.48E-09	0.41	27.41	1.69E-09	-0.34	0.75	0.064
4	0.403	4.87E-09	0.41	24.33	1.49E-09	-0.33	0.75	0.057
6	0.403	4.25E-09	0.40	21.25	1.29E-09	-0.33	0.75	0.049
8	0.403	3.64E-09	0.40	18.18	1.10E-09	-0.33	0.75	0.042

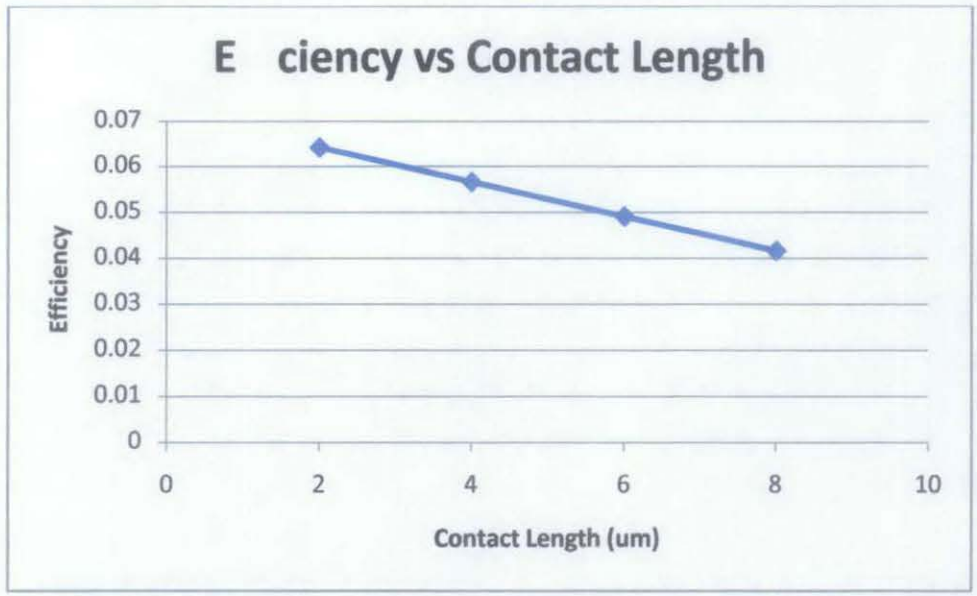

Figure 27: Metal Contact Length Variation Effects on the Efficiency.

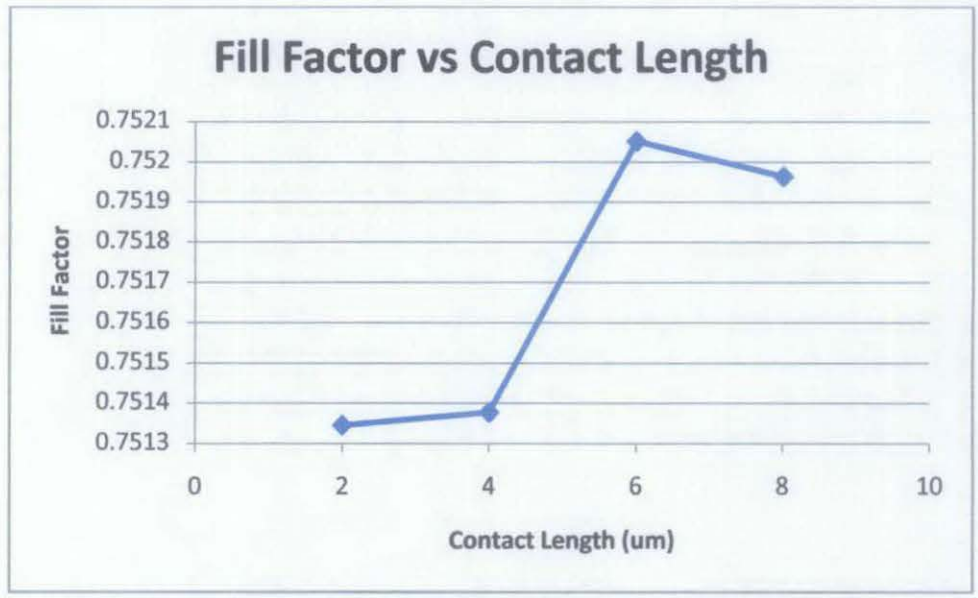

Figure 28: Metal Contact Length Variation Effects on the Fill Factor.

From the photogeneration analysis, the region right under the metal contact has poor photogeneration rate because the beam does not reach the region. When the metal contact width is increased, the poor photogeneration region also increases. This results into poor Efficiency of the solar cell.

4.2 Determination of the Complex Refractive Index

In order to fabricate the various particle size of the TiO_2 in the TiO_2/dye layer, the calcination temperature of the TiO_2 is varied. From the FE-SEM images, the

diameter of the TiO_2 is measured. The relation between the calcination temperature and TiO_2 particle size is tabulated in Table 9. The absorbance data which is obtained from the UV-Vis Absorption Spectroscopy measurement is as in Figure 29.

Table 9: Calcination temperature and the respective TiO_2 particle sizes.

Calcination Temperature, °C	TiO_2 Particle Size (nm)
400	12
500	20
600	25
700	30

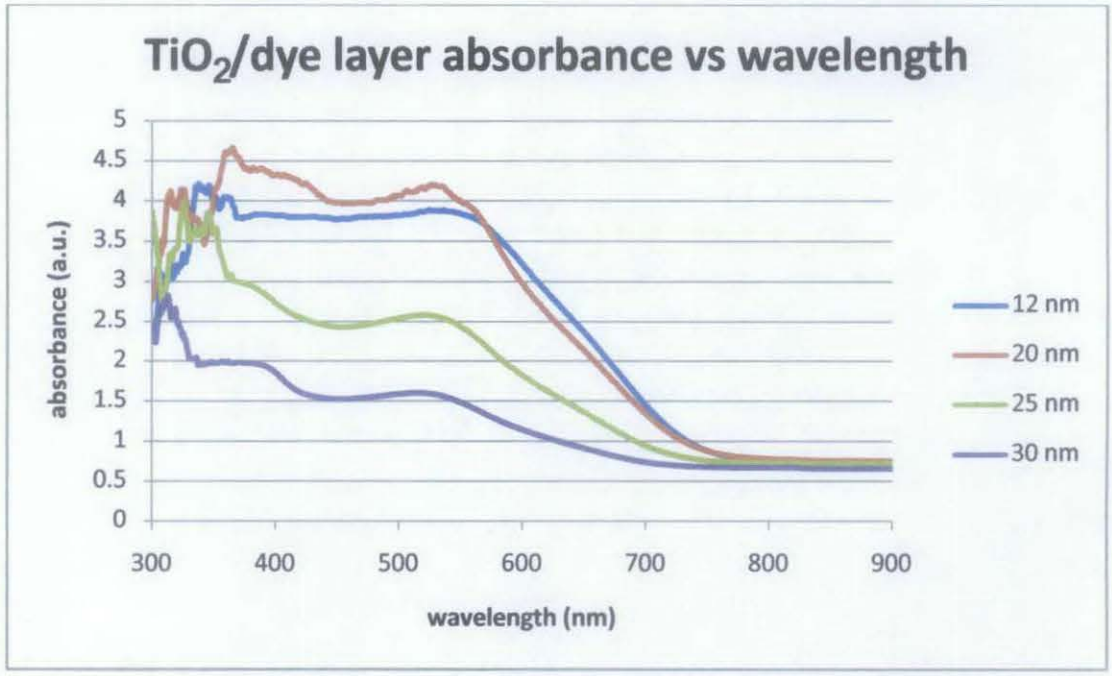

Figure 29: Absorbance of TiO_2/dye layer as a function of wavelength.

From the absorbance data of the TiO_2, the absorption coefficient is determined by using the relation as in equation 4. The result of the calculation is plot and shown in Figure 30.

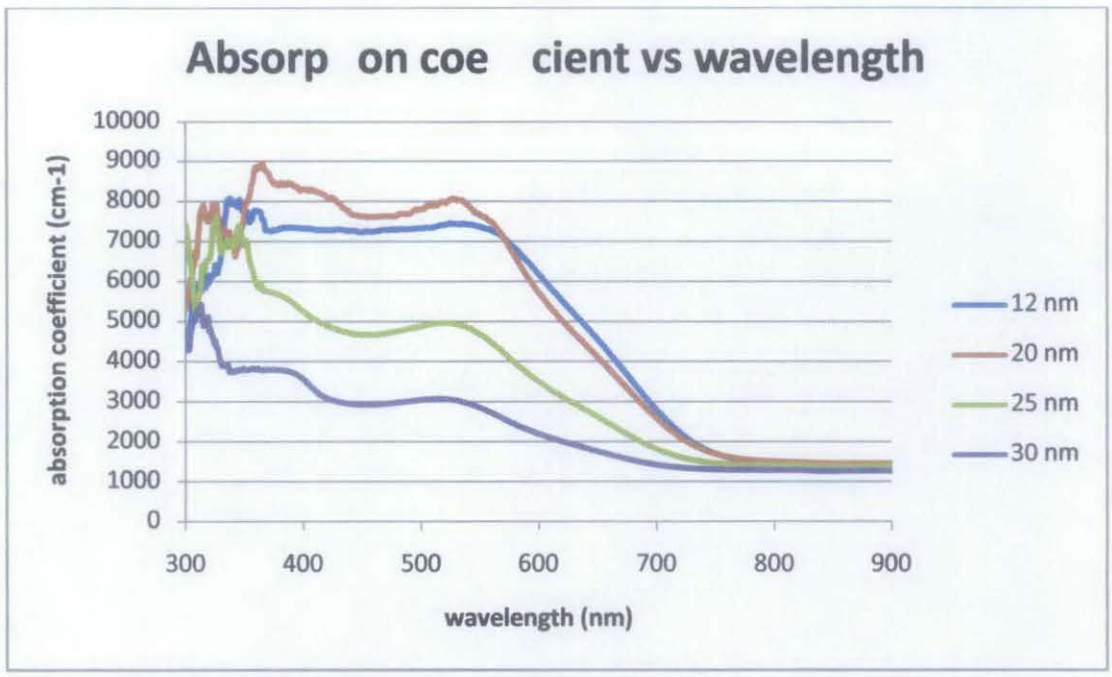

Figure 30: Absorption coefficient of TiO_2/dye layer as a function of wavelength.

Next, the absorption coefficient is used to obtain the extinction coefficient by using equation 6. Also, the refractive index is obtained through Kramers-Kronig relation. The Kramers-Kronig relation is being calculated by using the MATLAB programming. The extinction coefficient and refractive index is shown in Figure 31 and 32 respectively.

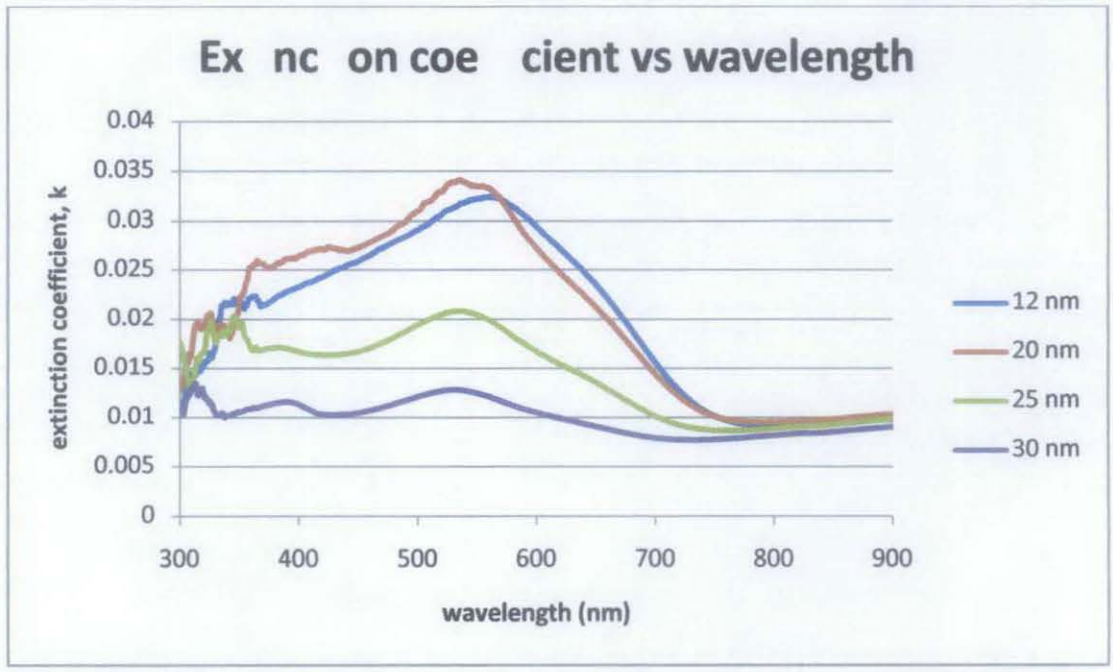

Figure 31: Extinction coefficient of TiO_2/dye layer as a function of wavelength.

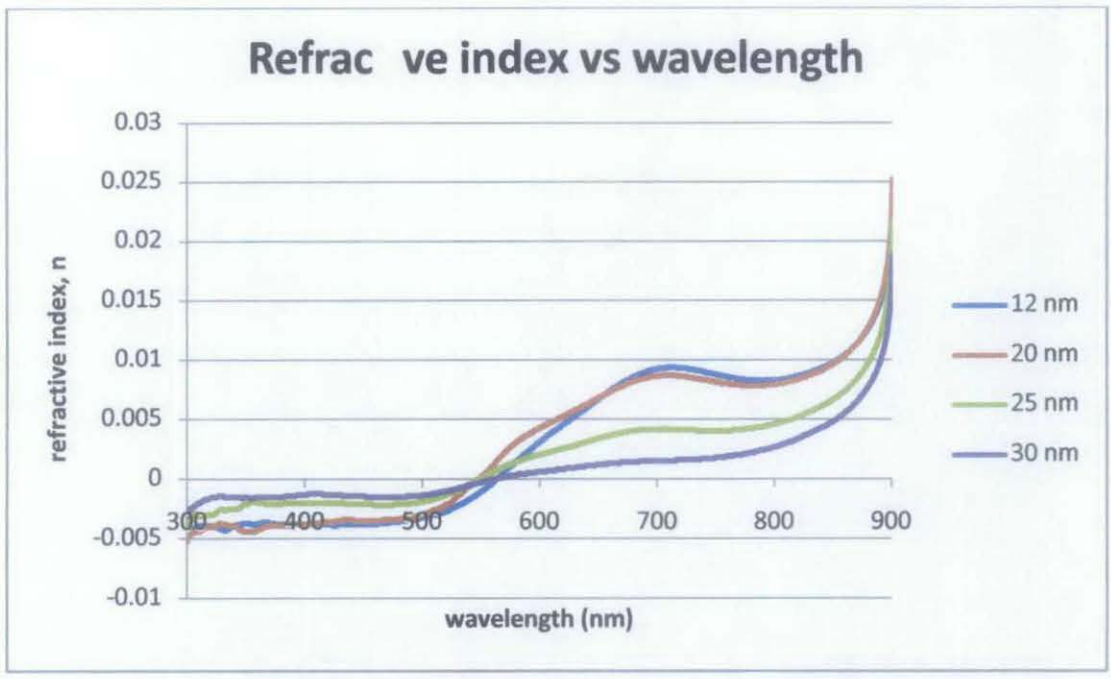

Figure 32: Refractive index of TiO_2/dye layer as a function of wavelength.

The steps used to obtain the complex refractive index for the TiO_2/dye layer is repeated for the electrolyte layer. The result of the measurement and calculation is shown in Figure 33 to 36.

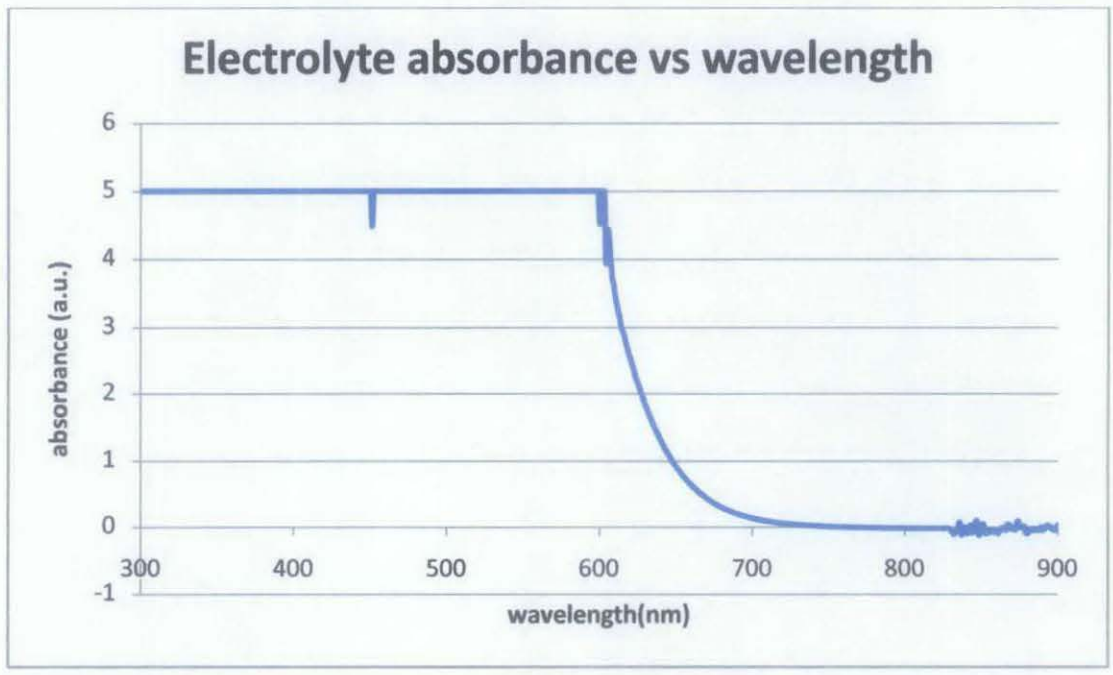

Figure 33: Absorbance of electrolyte as function of wavelength.

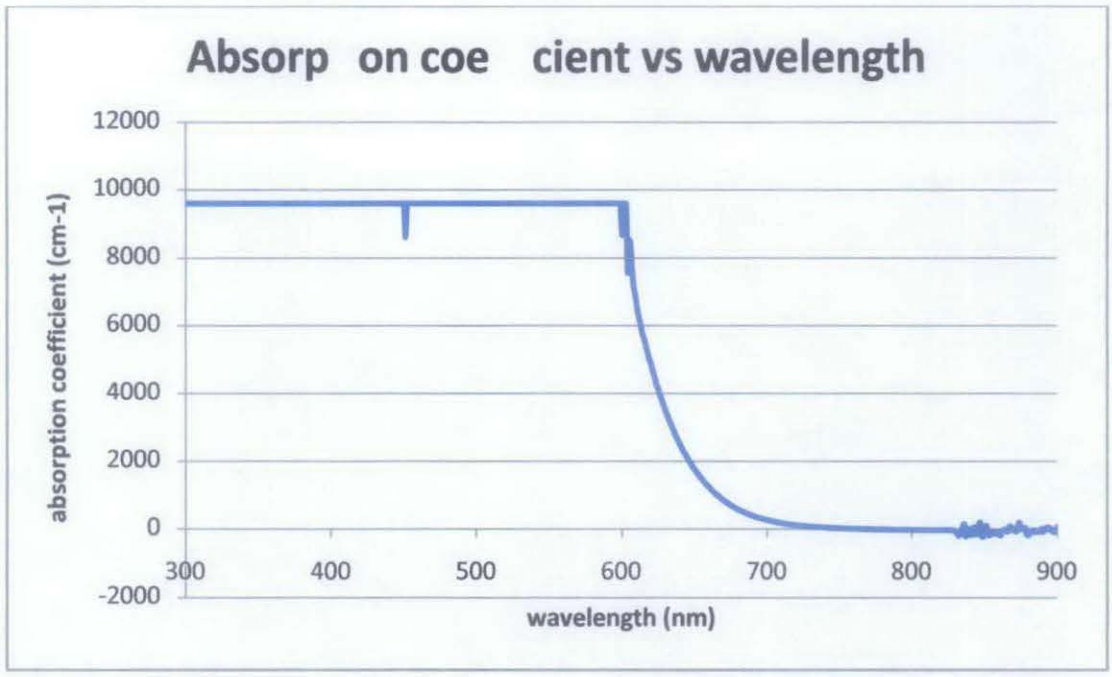

Figure 34: Absorption coefficient of electrolyte layer as a function of wavelength.

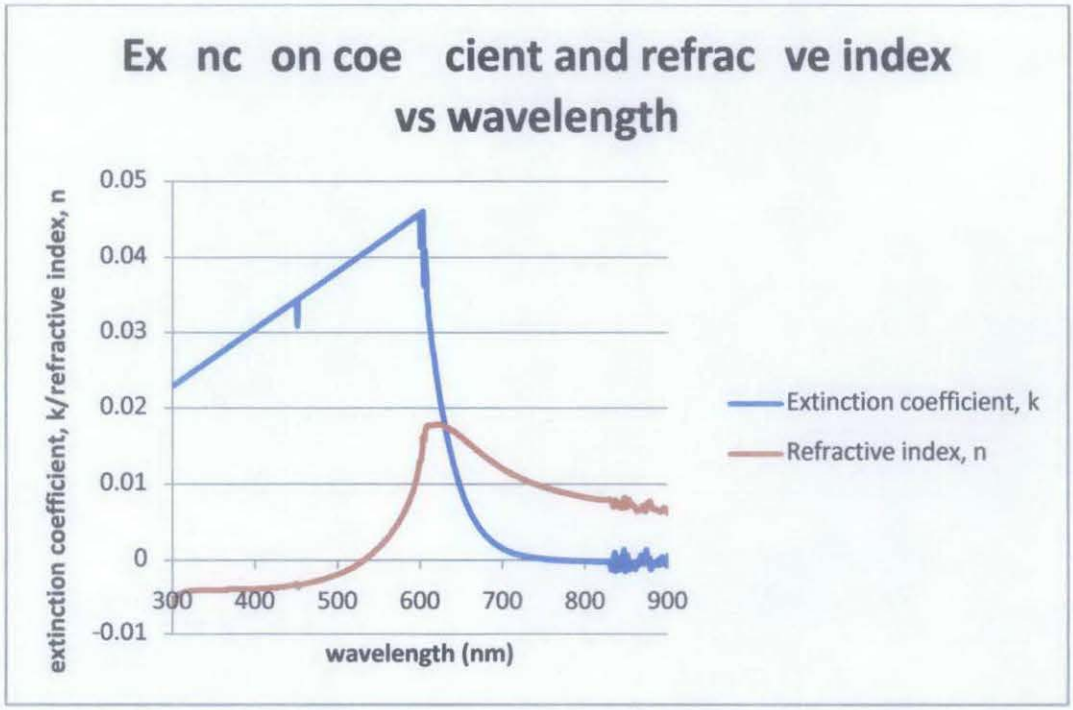

Figure 35: Extinction coefficient and refractive index of the electrolyte layer as a function of wavelength.

4.3 Dye-Sensitized Solar Cell Parameter Variation.

The Dye-Sensitized Solar Cell model which has been developed was used to simulate the effect of TiO_2 particle size. The simulation was varied by defining the variations in the complex refractive index of the TiO_2/dye layer. The simulation

results are compared with the measurement data from actual solar cell and shown from Figure 36 to Figure 41. The open circuit voltage, Voc of the DSSC shown in Figure 36 suggest that the optimum particle size for TiO_2 is at 20 nm. Meanwhile, Figure 37 and Figure 38 also show that the maximum point occurred at TiO_2 particle size of 20 nm. However, the voltage at maximum power point is not affected by the TiO_2 particle size.

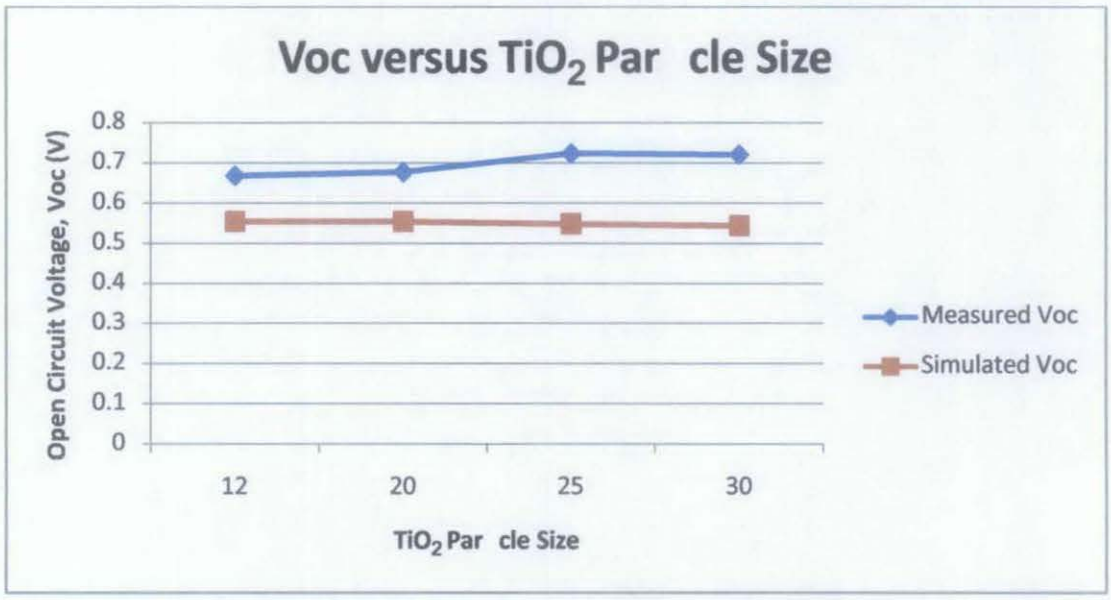

Figure 36: Effect of TiO_2 particle size variation on the open circuit voltage, Voc of the DSSC.

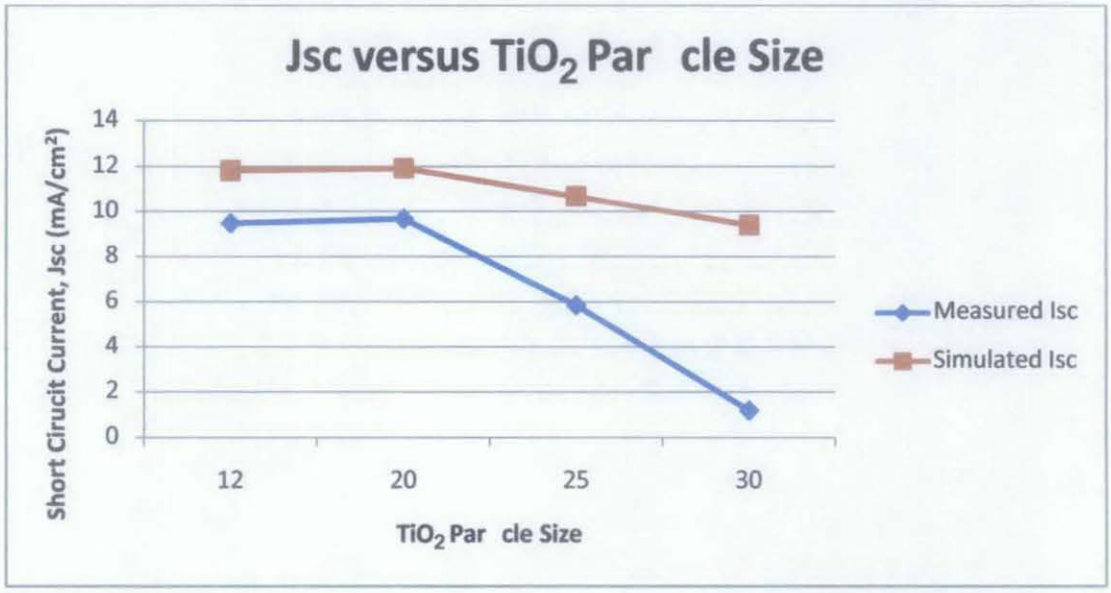

Figure 37: Effect of TiO_2 particle size variation on the short circuit current, Jsc of the DSSC.

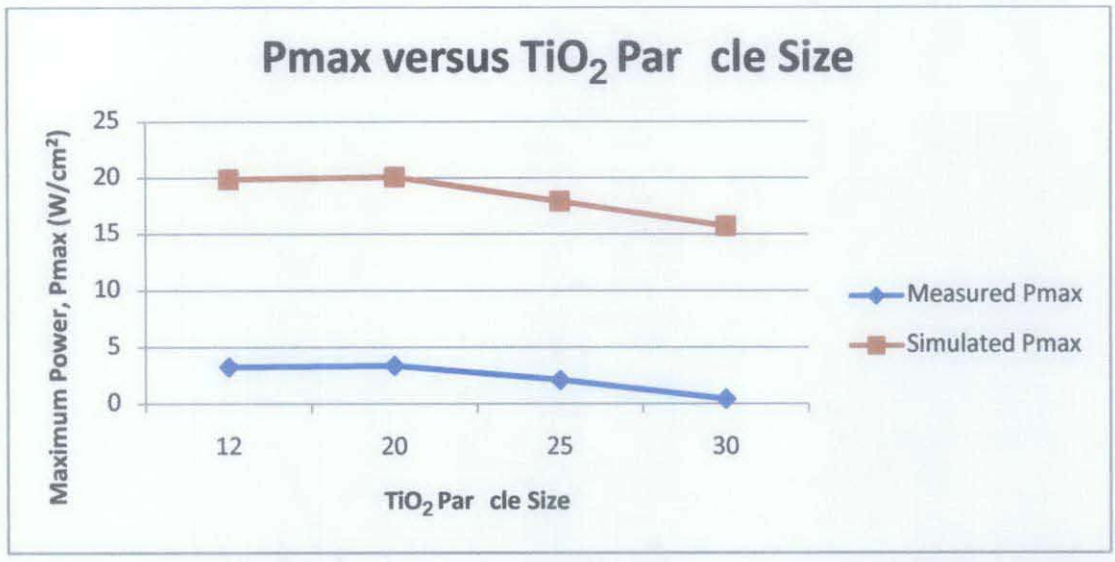

Figure 38: Effect of TiO_2 particle size variation on the maximum power, Pmax of the DSSC.

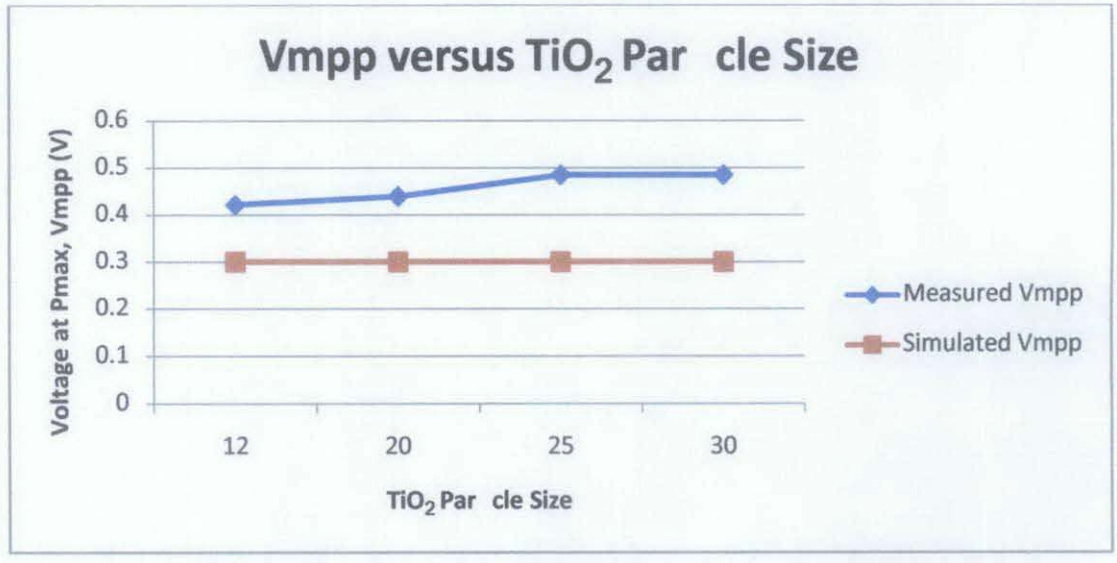

Figure 39: Effect of TiO_2 particle size variation on the corresponding voltage value when power is at maximum.

The maximum short circuit current, Jsc and open circuit voltage, Voc which occurred at TiO_2 particle size of 20 nm affected the Fill Factor, FF as shown in Figure 40. The figure shows that the Fill Factor is minimum at TiO_2 particle size of 20 nm. This is due to the reduction of the ratio of the maximum power to the product of open circuit voltage and short circuit current. However, the efficiency of the DSSC is maximum on TiO_2 particle size of 20 nm as shown in Figure 41.

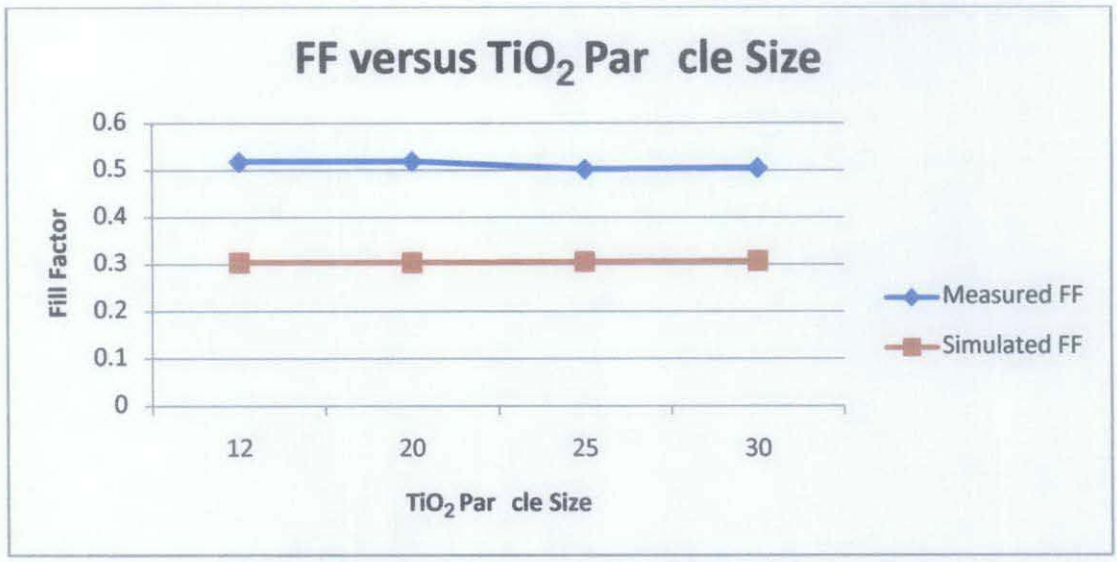

Figure 40: Effect of TiO_2 particle size variation on the Fill Factor, FF.

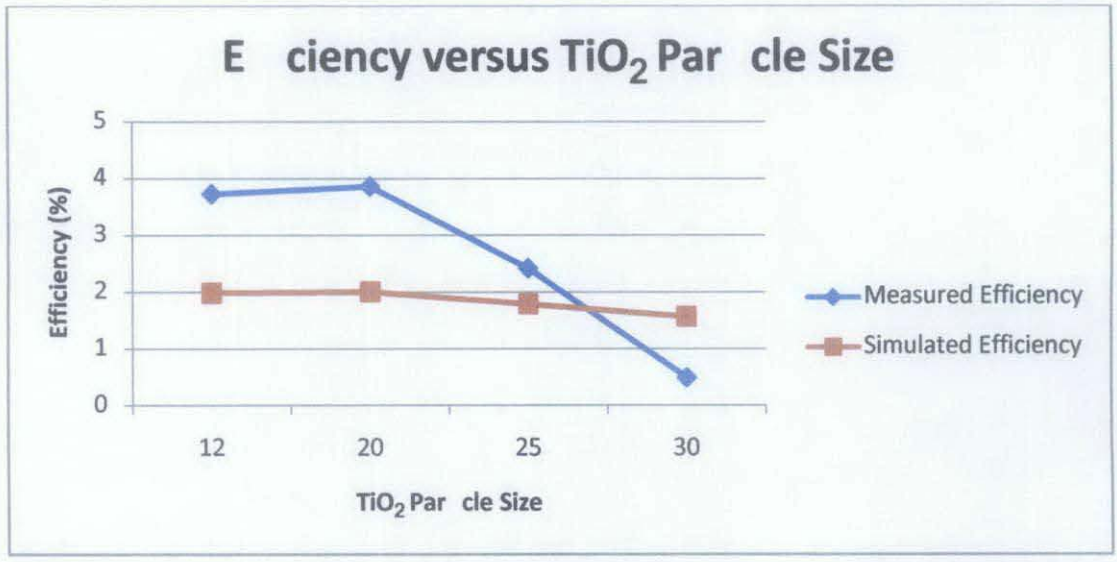

Figure 41: Effect of TiO_2 particle size variation on the efficiency of DSSC.

Although there are variations from the measurement data and simulation data, the effects of the particle size variation are able to be identified. The simulation data suggest that the optimum particle size is about 20 nm. This is because the particle size with larger diameter had better dye adsorption for increased electron hole generation [16]. The improved dye adsorption is caused by higher crystallinity and pore size which lead to increase in efficiency [9].

CHAPTER 5

CONCLUSION AND RECOMMENDATION

5.1 Conclusion

The student was familiarized by simulating the efficiency of the P-N junction solar cell. From the familiarization process, the parameters variation for P-N junction solar cell have shown that only certain parameters would produce a significant change in the short circuit current, Jsc and open circuit voltage, Voc and hence effect the efficiency of the solar cell. The Boron doping concentration plays a more important role than the Phosphorus doping concentration. This is because Boron doping concentration increases the efficiency and the Fill Factor of the solar cell significantly; meanwhile the Phosphorus doping concentration only present slight changes to the efficiency and the Fill Factor.

It is also important to make sure the oxide layer is very thin in order to increase the absorbed sunlight. This is because the P-N junction solar cell is not efficient when operated under diffused light. The metal contact is length is also important in order to produce an efficient solar cell. From the simulation, the least length of the metal contact will produce a more efficient solar cell. However, the metal contact length does not play a major role to affect the Fill Factor.

The data which is collected for P-N Junction solar cell shows that Boron doping concentration, oxide layer thickness and metal contact length play a major role in increasing the efficiency of the solar cell. However, the efficiency of the solar cell is not varied significantly when the Phosphorus doping concentration is increased.

Next, the student has determined the complex refractive index of the materials used in Dye-Sensitized Solar Cell. The results of the calculated refractive index have shown the effect of the particle size variation. The complex refractive index for

particle size of 12 and 20 nm is closely varied however; the complex refractive index for 25 and 30 nm shows large variation from the other data.

Lastly, the DSSC with TiO_2 particle size varied is simulated using ATLAS. The simulation has been able to show the pattern of the effects of variations in TiO_2 particle size. From the simulation and the measurement of the IV characteristics of the Dye-Sensitized Solar Cell, the optimum particle size for titania is in the range of 20 nm.

5.2 Recommendation

From the literature, the open circuit voltage, Voc of the Dye-Sensitized Solar Cell is the difference of the Fermi level of the semiconducting oxide and the energy level of the redox mediator. Hence, future work should include in adjusting the Fermi level of the redox mediator so that the open circuit voltage value can be improved. Comparing the result of the simulation with the measured IV characteristics shows that the particle size of titania in the titania/dye layer does not only affect the absorption of the dye. Hence, other parameters such as the effective electron mobility need to be considered to in order to improve the result of the simulation.

REFERENCE

[1] Andrzej Graja (1994), Optical Properties. In Jean-Pierre Farges (1994), Organic Conductors: Fundamentals and Application. New York: Marcel Dekker Inc.

[2] Carl W. Garland, Joseph W. Nibler, David P. Shoemaker (2009), Experiments in Physical Chemistry, 8th Ed.McGrawhill Companies.

[3] Hubert Cachet (2005), Films and Powers of Fluorine Doped Tin Dioxide. In T Nakajima & H Groult (2005), Fluorinated Materials forEnergy Conversion. Elesevier Ltd.

[4] John Perlin (2004), The Silicon Solar Turns 50. National Renewable Energy Laboratory. Retrieved from http://www.nrel.gov/docs/fy04osti/33947.pdf

[5] Janne Halme, Paula Vahermaa, Kati Miettunen, Peter Lund (2010), Device Physics of Dye Solar Cells. Review "Advance Energy Materials", vol. 22, issue 35, pp. E210-E234.

[6] Jeffery L. Gray (2003), The Physics of the Solar Cell. In Antonio Luque & Steven Hegedus, *Handbook of Photovoltaic Science and Engineering*. West Sussex: John Wiley & Sons Ltd.

[7] K.R. Catchpole & M.A. Green (2002), Third Generation Photovoltaics. Conference on Optoelectronic and Microelectronic Materials and Devices (2002).

[8] K.L. Chopra, P.D. Paulson and V. Dutta (2004), Thin-Film Solar Cells: An Overview. Progress in Photovoltaics: Research and Application (2004).

[9] Katrin Wessels, Melanie Minnermann, Jiri Rathousky, Michael Wark & Torsten Oekermann (2008), Influence of Calcination Temperature on the Photoelectrochemical and Photocatalytics Properties of Porous TiO_2 Films

Electrodeposited from Ti(IV)-Alkoxide Solution. J. Phys. Chem. C 2008, 112, 15122-15128.

[10] L.J.A. Korster, E.C.P. Smits, V.D. Mihailetchi and P.W.M. Blom (2005), Device Model for the Operation of Polymer/Fullerene Bulkheterojunction Solar Cells. Physical Review.

[11] Martin A. Green (2001), 'Crystalline Silicon Solar Cell'. In Mary D Archer & Robert Hill, *Clean Electricity from Photovoltaics*. London : Imperial College Press.

[12] Michael Gratzel (2006), 'Nanocrystalline Injection Solar Cells'. In Jef Poortmans & Vladimir Arkhipov, *Thin Film Solar Cells: Fabrication, Characterization and Application*. West Sussex: John Wiley & Sons Ltd.

[13] R.Konenkamp, I. Rieck (2000), Electrical Properties of Schottky Diodes on nano-porous TiO_2 Films. Material Science & Engineering B. Elsevier Science S.A.

[14] S. Michael, A.D. Bates & M.S. Green (2005), Silvaco ATLAS as a Solar Cell Modelling Tool. Conference Record of the Thirty-first IEEE Photovoltaic Specialists Conference (2005).

[15] Stephen J. Fonash (2010), Solar Cell Device Physics, 2nd Edition. Elsevier Inc.

[16] TammyP. Chou, Qifeng Zhang, Bryan Russo, Glen E. Fryxell, and Guozhong Cao (2007), Titania Particle Size Effect on the Overall Performance of Dye-Sensitized Solar Cells. J. Phys. Chem. C 2007, 111, 6296-6302.

[17] T.Meier, P.Thomas & S.W. Koch.(2007), Coherent Semiconductor Optics: From Basic Concepts to Nanostructure Applications. Berlin; New York: Springer.

APPENDIX A: GANTT CHART

Activities	FINAL YEAR PROJECT I													
	W1	W2	W3	W4	W5	W6	W7	W8	W9	W10	W11	W12	W13	W14
Review on Solar Cell Technology Development														
P-N Junction Solar Cell Simulation on ATHENA and ATLAS														
Solar Cell Parameter Variation														
Analysis of Findings and Report Writing														

Activities	FINAL YEAR PROJECT II													
	W1	W2	W3	W4	W5	W6	W7	W8	W9	W10	W11	W12	W13	W14
Absorption Spectroscopy of DSSC														
DSSC Simulation on ATLAS														
Variation of Titania Particle Size														
Analysis of Findings and Report Writing														

APPENDIX B: ATLAS CODING FOR DSSC

```
go atlas simflags="-P 1"
mesh width=1e12

x.mesh l=0.00 s=0.5
x.mesh l=1.00 s=0.5
y.mesh l=0.00  s=0.05
y.mesh l=12.00  s=0.05
y.mesh l=37.00  s=0.05

region number=1 user.material=BulkLayer y.min=0.00 y.max=12.00
region number=2 user.material=REDOX y.min=12.00 y.max=37.00

electrode name=anode   top
electrode name=cathode bottom

contact num=1 workf=4.4
contact num=2 workf=4.4

model langevin singlet s.dissoc
model print

material material=BulkLayer user.default=Organic
user.group=Semiconductor
material material=REDOX user.default=Organic
user.group=Semiconductor

material material=BulkLayer permi=50 affinity=4.0 eg300=1.5 \
      nc300=2.8e19 nv300=1e19
material material=REDOX permi=3.5 affinity=3.4 eg300=1.8 \
      nc300=2.8e19 nv300=1e19

material material=BulkLayer index.file=dye400.nk
material material=REDOX index.file=iodide.nk

material material=REDOX qe.exciton=1.0
material material=REDOX knrs.exciton=1.82694e6 lds.exciton=0.0
\
         taus.exciton=1.0e20 rst.exciton=1.0
material material=REDOX a.singlet=2 s.binding=0.004

mobility material=BulkLayer mun=0.3 mup=450e-4
mobility material=REDOX mun=1350 mup=450

save outf=check1.str

beam num=1 x.origin=0.5 y.origin=-2.0 angle=90.0 AM1.5

output band.par con.band val.band e.mob h.mob opt.int

probe name=inten beam=1 intensity
```

```
method climit=1e-4 maxtrap=0

#IV Characteristics
solve init
solve previous
log outfile=dark_current.log
solve vcathode=-1 vstep=0.05 vfinal=1 name=cathode
log off

solve init
solve prev
solve b1=1
log outf=light_current.log
solve vcathode=-1 vstep=0.05 vfinal=1 name=cathode b1=1
log off

save outf=check2.str

extract init infile="light_current.log"
extract name="Isc" y.val from curve(v."cathode",
(i."cathode")) where x.val=0
extract name="Voc" x.val from curve(v."cathode",
(i."cathode")) where y.val=0
extract name="Jsc (mA/cm2)" abs($"Isc")*1e-1
extract name="Power" curve(v."cathode", (v."cathode" *
i."cathode" *(-1))) \
        outf="P.dat"
extract name="Pmax" max(curve(v."cathode",
(v."cathode"*i."cathode"*(-1))))
extract name="V_Pmax" x.val from
curve(v."cathode",(v."cathode"*i."cathode")) \
        where y.val=(-1)*$"Pmax"
extract name="Fill Factor" ($"Pmax"/(abs($"Isc")*$"Voc"))
extract name="intens" max(probe."inten")
extract name="Eff" (($Pmax/($"intens"*1e4))*100)

tonyplot dark_current.log -overlay light_current.log
tonyplot P.dat
tonyplot check2.str

quit
```